TECHNICAL MEMORANDUM

X-293

X 623 4-17-62

INVESTIGATION OF AERODYNAMIC CHARACTERISTICS AT HIGH SUBSONIC SPEEDS OF TWO SUPERSONIC-CRUISE AIRPLANE CONFIGURATIONS HAVING TAIL SURFACES OUTBOARD OF THE WINGTIPS

By Paul G. Fournier and William C. Sleeman, Jr.

Langley Research Center
Langley Field, Va.

NATIONAL AERONAUTICS AND SPACE ADMINISTRATION
WASHINGTON

August 1960

NATIONAL AERONAUTICS AND SPACE ADMINISTRATION

TECHNICAL MEMORANDUM X-293

INVESTIGATION OF AERODYNAMIC CHARACTERISTICS AT HIGH SUBSONIC SPEEDS OF TWO SUPERSONIC-CRUISE AIRPLANE CONFIGURATIONS HAVING TAIL SURFACES OUTBOARD OF THE WINGTIPS*

By Paul G. Fournier and William C. Sleeman, Jr.

SUMMARY

12797

The aerodynamic characteristics at high subsonic speeds of two outboard-tail airplane configurations have been investigated in the Langley high-speed 7- by 10-foot tunnel over a Mach number range from 0.40 to 0.94. The models had the horizontal and vertical tail surfaces mounted on slender bodies attached to the tips of a low-aspect-ratio highly sweptback wing. One model had a 70° sweptback wing which had both twist and negative dihedral, and the other model had a 60° sweptback wing which had no twist or dihedral. Both models had simulated engine installations attached which represented a six-engine arrangement having a common air inlet with air flow through the inlet. The static longitudinal and lateral stability and control characteristics were obtained over an angle-of-attack range from about -2° to 24°.

Comparison of the pitching-moment characteristics at subsonic speeds for the two outboard-tail models tested with the characteristics of these models at supersonic speeds indicated that the overall low-lift static-margin increase was about 9 percent of the mean aerodynamic chord when the Mach number was increased from 0.60 to 3.0. The static margin at low lift was, however, very low at subsonic speeds for both models. The variation of pitching moment with lift indicated a large loss of stability for lift coefficients above about 0.35, and results for both models showed static longitudinal instability above an angle of attack of about 9°. Values of maximum lift-drag ratio for the model having a 70° sweptback wing were somewhat higher at a Mach number of 0.60 than values for the model having a 60° sweptback wing; however, near a Mach number of 0.90 maximum lift-drag ratios for the two models were about the same. The maximum lift-drag ratios obtained were approximately 7.65 and 8.15 for the 60° and 70° sweptback-wing models, respectively. The static directional stability of both models was fairly high at low angles of attack and became very high as the angle of attack increased to 24°.

Drobka

*Title, Unclassified.

INTRODUCTION

The National Aeronautics and Space Administration has done much work toward achieving airplane configurations having high values of lift-drag ratio and adequate stability at the design cruise Mach number of 3.0. One of the types of configurations investigated had its tail surfaces mounted on slender bodies attached to the tips of a low-aspect-ratio highly sweptback wing. Test results at supersonic speeds for two outboard-tail models are presented in references 1 to 3 and results of some general studies at low speed showing effects of wing sweep and horizontal-tail size are presented in reference 4.

The purpose of the present investigation was to obtain the aerodynamic characteristics at high subsonic speeds of the same outboard-tail models used in the tests at supersonic speeds reported in references 1 and 2. The subsonic tests were conducted in the Langley high-speed 7- by 10-foot tunnel over a Mach number range from 0.40 to 0.94 and for an angle-of-attack range from -2° to 24°. Static longitudinal and lateral stability and control characteristics were studied over the test Mach number range. A few tests were made to assess the lateral and directional control characteristics of the models.

SYMBOLS

The data of this investigation are presented with respect to the system of axes shown in figure 1. The lateral characteristics are referred to the body axes and the longitudinal characteristics are referred to the stability axes. Moment coefficients are given about a moment-reference point located at 65 percent of the mean aerodynamic chord of the wing alone (excluding the tails) for model 1 and at 56.12 percent of the mean aerodynamic chord of the wing alone for model 2. These moment-reference points are the same as those used at supersonic speeds for the models of references 1 and 2. The coefficients are based on the geometry of the composite plan form of the wing plus the horizontal tail surfaces inasmuch as the tail would provide positive lift for trimmed flight.

C_D external-flow drag coefficient, $\frac{\text{Total drag}}{qS} - (C_{D,b} + C_{D,c} + C_{D,i})$

$C_{D,b}$ engine-pack base drag coefficient, $\frac{\text{Base drag}}{qS}$

$C_{D,c}$ balance-chamber drag coefficient, $\frac{\text{Chamber drag}}{qS}$

$C_{D,i}$ engine-pack internal-flow drag coefficient, $\frac{\text{Internal drag}}{qS}$

C_L lift coefficient, $\frac{\text{Lift}}{qS}$

C_m pitching-moment coefficient, $\frac{\text{Pitching moment}}{qS\bar{c}}$

C_l rolling-moment coefficient, $\frac{\text{Rolling moment}}{qSb}$

C_n yawing-moment coefficient, $\frac{\text{Yawing moment}}{qSb}$

C_Y side-force coefficient, $\frac{\text{Side force}}{qS}$

$$C_{l_\beta} = \left(\frac{\Delta C_l}{\Delta \beta}\right)_{\beta=\pm 4^\circ}$$

$$C_{n_\beta} = \left(\frac{\Delta C_n}{\Delta \beta}\right)_{\beta=\pm 4^\circ}$$

$$C_{Y_\beta} = \left(\frac{\Delta C_Y}{\Delta \beta}\right)_{\beta=\pm 4^\circ}$$

b span of wing plus horizontal tail, ft

c chord length in free-stream direction, ft

$\bar{c}$ mean aerodynamic chord of wing plus horizontal tail, ft

S area of wing plus horizontal tail, including wing-body intercept (wingtip and tail-root chords are assumed to lie on the center line of the wingtip bodies) but not including area of wing trailing-edge extensions, sq ft

q free-stream dynamic pressure, lb/sq ft

M free-stream Mach number

α angle of attack referred to fuselage reference line, deg

β angle of sideslip referred to fuselage center line, deg

δ_r rudder deflection relative to chord plane of vertical tail (positive when trailing edge is deflected to left), deg

i_t horizontal-tail incidence angle relative to center line of rear half of wingtip bodies (positive when trailing edge is down), deg

L/D lift-drag ratio, C_L/C_D

Subscript:

max maximum

Model component designations:

W wing

B fuselage

E engine pack

O wingtip bodies

V vertical tails

H horizontal tail

F ventral fins

APPARATUS AND MODELS

The tests were conducted in the Langley high-speed 7- by 10-foot tunnel on two outboard-tail models. The forces and moments acting on the models were measured by means of a six-component internal strain-gage balance. The balance was attached to a variable-angle sting support system which was remotely operated.

Description of Model 1

The configuration designated as model 1 is shown in figure 2 and is the same model used in the investigation reported in reference 1. Photographs of model 1 are given in figure 3 and the geometric characteristics

are summarized in table I. The cross section of the fuselage was basically semicircular from the nose rearward for about 22 inches and faired smoothly from this point to a circular base. A detachable engine pack representing a three-over-three clustered engine arrangement was mounted beneath the model fuselage. (See fig. 2(b) for details of the engine pack.) This pack consisted of a two-dimensional split inlet ducted to exhaust through three nozzles. An integral part of the pack was the wedge-type boundary-layer diverter located on the upper surface of the inlet-duct housing. The design Mach number for the engine pack was 3.0 and no modifications were made to the engine pack for subsonic operation.

The wing of model 1 had 70° of sweep at the leading edge, an aspect ratio of 1.0, a taper ratio of 0.3919, and a dihedral angle of -5.3°. The wing had NACA 65A004 airfoil sections and was twisted about the 0.50-chord line so that it had -2.8° twist at the tip and the theoretical root chord was located on the fuselage reference line at 0° incidence. The wingtip bodies were attached with the center line coincident with the wingtip chord and were therefore inclined nose down 2.8° with respect to the fuselage reference line. Inasmuch as the stabilizer settings given in this report are referred to the center line of the wingtip body, the inclination of this body must be subtracted from the stabilizer settings given in order to determine the setting relative to the fuselage reference line, which is the more commonly used definition.

The horizontal and vertical tails were swept back 60° at the leading edge and had a panel aspect ratio of 0.9185, a taper ratio of 0.3069, and NACA 65A003 airfoil sections. The vertical tails were alined on the wingtip bodies so that the tails had 1.5° of toe-out. (See plan view, fig. 2(a).) A wing trailing-edge extension was tested on the model and details of this extension are given in figure 2(c). A ventral fin which was attached to each wingtip body for a few tests is shown in figure 2(d).

Description of Model 2

A drawing of model 2 is given in figure 4 and this model is the same model used in the investigations of references 2 and 3. Photographs of model 2 are given in figure 5 and the geometric characteristics are summarized in table II. The forward part of the fuselage of the model had a cross-sectional shape composed of two semiellipses having their major axes horizontal and coincident. The minor axes of these semiellipses were selected so that the height of the body was one-half of the width. Most of the rear portion of the body was composed of a semicircular shape with its diameter located on the bottom surface of the wing. The engine pack used on model 2 was designed for operation at $M = 3.0$ and was similar to that used on model 1 except that the internal flow was discharged through four exits, and the engine pack could not be removed for

tests of the model alone since the strain-gage balance was mounted in the engine pack.

The wing of model 2 had 60° of sweep at the leading edge, an aspect ratio of 0.90, a taper ratio of 0.6654, and $2\frac{1}{2}$-percent-chord-thick hexagonal airfoil sections with ridge lines at 1/3- and 2/3-chord lines. The wing was not twisted and had no dihedral or incidence. The outer bodies attached to the wingtips had a 1.2 to 1.0 elliptical cross section with the major axis vertical. The center line of the forward half of the wingtip bodies was parallel to the wing-chord plane, whereas the center line of the rear half was inclined upward 3°. (See fig. 4(a).) The wingtip bodies were "bent" in order to have the horizontal tail surfaces alined with the bodies at the trim setting for design conditions at a Mach number of 3 when used on the untwisted wing of model 2. These bodies were also bent inward at the rear so that the vertical tail surfaces which were alined with the bodies would have 1.5° of toe-out. (See plan view, fig. 4(a).)

L 8 8 7

The horizontal tail surfaces used on model 2 were swept 61.5° at the leading edge and had a panel aspect ratio of 1.0392, a taper ratio of 0.2500, and $2\frac{1}{2}$-percent-chord-thick hexagonal airfoil sections. The vertical tails were swept 52° at the leading edge and had an aspect ratio of 0.7479, a taper ratio of 0.2500, and $2\frac{1}{2}$-percent-chord-thick double-wedge airfoil sections. The tail surfaces were considered to be undeflected when they were alined with the center lines of the rear part of the wingtip bodies. The wing trailing-edge extension used on model 2 extended rearward from the wing trailing edge at approximately the 3° inclination of the rear part of the outer body (see figs. 4 and 5) and was on the model for all tests. The total exposed plan-form area of both extensions was 0.115 square foot; however, this added area was not used in the reference area for the reduction of data to coefficients.

TESTS

Tests of model 1 and model 2 were conducted over an angle-of-attack range from approximately -2° to 24° for model 1 and from -2° to 16° for model 2. The test Mach number range extended from 0.60 to 0.94 for model 1 and generally from 0.40 to 0.90 for model 2. Both the lower Mach number range and the reduced angle-of-attack range used for model 2 were necessitated by the rearward location of the strain-gage balance in model 2. Some test results were obtained on model 2 in which the Mach number extended to 0.94 for the zero-lift condition in order to obtain

the drag. The test Reynolds number range, based on the wing mean aerodynamic chord, was 4.0×10^6 to 5.0×10^6 for model 1 and 3.7×10^6 to 6.0×10^6 for model 2.

Transition was fixed on both models by means of roughness strips placed around the fuselage and wingtip bodies about 2 inches behind the noses and along a constant-percent-chord line (upper and lower surfaces) on the wings and tail surfaces. For model 1 the roughness on wing and tails was along the 10-percent-chord line and for model 2 the roughness was along the 5-percent-chord line. The roughness on model 1 was formed by No. 60 carborundum in a strip 1/32 inch wide having about 50 grains per inch of strip. Roughness on model 2 was formed by placing single grains of sand having a nominal size of 0.018 inch along the transition line at a spacing of approximately 1/32 inch between grains. Transition was fixed for both models except for a few tests of model 1 to determine effects of fixing transition.

Longitudinal characteristics of the models were obtained at each Mach number at 0° sideslip through the angle-of-attack range. Lateral-stability derivatives were obtained from tests of the models in which the angle of attack was varied at fixed sideslip angles of $\pm 4^\circ$. A few tests were conducted on model 1 in which the sideslip was varied and the angle of attack held constant.

CORRECTIONS

Jet-boundary corrections to the angle of attack and drag coefficients, and blockage corrections to the dynamic pressure have been determined by standard procedures and these corrections were applied to the basic data. In addition, the drag coefficients have been corrected for effects of tunnel buoyancy. The angles of attack and sideslip have been corrected for deflection of the sting and balance under load.

The drag data for both model 1 and model 2 have been adjusted to correspond to free-stream static pressure acting on the entire base of the model including the area occupied by the sting but not including the duct exit areas. Pressures measured in the balance chamber and over the engine-pack base were used to obtain base-pressure corrections by application to the appropriate areas. The drag data for the models have also been corrected for internal-flow drag by subtracting $C_{D,i}$ (force coefficient computed from duct exit pressures obtained by a total pressure survey and static orifices and by using a standard momentum-balance equation) from the measured drag data. These drag

corrections applied to the data of both models are presented in figure 6. No corrections have been applied to the data of either model 1 or model 2 to account for drag of the engine-pack boundary-layer diverter.

PRESENTATION OF RESULTS

The basic test results for model 1 are given in figures 7 to 18 and results for model 2 are presented in figures 19 to 23. Some results are summarized in figures 24 to 27. An outline of the content of the data figures is as follows:

	Figure
Model 1	
Longitudinal characteristics:	
Effect of fixing transition	7
Effect of vertical tails and wingtip bodies	8
Effect of horizontal-tail incidence	9
Effect of horizontal-tail incidence on lift-drag ratios	10
Effect of wing trailing-edge extension	11
Lateral-stability derivatives:	
Effect of engine pack	12
Effect of vertical tails and ventral fins	13
Effect of wingtip bodies	14
Component contributions	15
Effect of vertical tails on characteristics in sideslip	16
Effect of horizontal-tail roll control	17
Effect of vertical-tail incidence	18
Model 2	
Effect of horizontal-tail incidence	19
Effect of vertical tails on lateral-stability derivatives	20
Contribution of vertical tails to lateral-stability derivatives	21
Effect of horizontal-tail roll control	22
Effect of rudder deflection	23
Summary Figures	
Effect of engine pack and horizontal tail on performance parameters of model 1	24
Effect of engine pack and horizontal tail on the longitudinal-stability parameters of model 1	25
Effect of horizontal tail on the performance parameters of model 2	26
Effect of horizontal tail on the longitudinal-stability parameters of model 2	27

SUMMARY OF RESULTS

A detailed discussion of results obtained in the investigation at high subsonic speeds of two outboard-tail models has been omitted in order to expedite publication of these data. A few observations are made, however, to point out some of the most important results obtained.

Longitudinal Characteristics

The pitching-moment data presented in this report for both model 1 and model 2 are referred to the same moment-reference point as was used in the data presentation for these models at supersonic speeds (refs. 1 and 2) in order to compare the present tests directly with the supersonic tests. The low-lift static margin at a Mach number of 3 was approximately 14 percent $\bar{c}$ for model 1 (ref. 1) and 10 percent $\bar{c}$ for model 2. The corresponding values of low-lift static margin at a Mach number of 0.60 were 5.2 percent $\bar{c}$ (fig. 25) and 1.0 percent $\bar{c}$ (fig. 27) which indicate that the overall static-margin increase, as M increased from 0.60 to 3.0, was only about 9 percent $\bar{c}$ for both of the outboard-tail models. The level of stability at $M = 3.0$ was, however, such that the 9-percent-$\bar{c}$ shift caused the subsonic stability near zero lift to be very low. The variation of pitching-moment coefficient with lift coefficient for both model 1 and model 2 (figs. 9 and 19) shows that a large loss of stability occurred for lift coefficients above about 0.35, and longitudinal instability was indicated for angles of attack of approximately 10° for model 1 and 8° for model 2. This loss of stability at moderate angles of attack was due to a loss in the tail contribution which was probably caused by relative movement of the horizontal tail below the region of maximum upwash as the model angle of attack increased. Methods for alleviating the longitudinal instability encountered on some outboard-tail configurations have been explored in tests at low speed (ref. 4) and a configuration was achieved which had no large losses in longitudinal stability over an angle-of-attack range extending to 30° (unpublished data).

Performance Parameters

The summary of performance parameters presented in figures 24 and 26 shows that addition of the outboard horizontal tail surfaces increased maximum lift-drag ratios for model 1 by a value of about 1.5 and for model 2 by a value of about 1.3. Maximum lift-drag ratios for model 1 decreased from a value of about 8.15 at $M = 0.60$ to a value of 7.45 at $M = 0.94$; whereas values for model 2 increased from 7.25 at $M = 0.40$ to a value of 7.65 at $M = 0.80$ and then decreased slightly as M increased

to a value of 0.90. Removal of the engine pack of model 1 (fig. 24) caused a substantial increase in maximum lift-drag ratios and values obtained without the engine pack increased as Mach number increased.

A comparison of maximum lift-drag ratios of model 1 and model 2 (figs. 24 and 26) shows about the same values near the highest test Mach number; however, the lift-drag ratios for model 1 were somewhat higher than those for model 2 near a Mach number of 0.60 even though the minimum drag of model 2 was lower than that for model 1 throughout the Mach number range. There are many significant geometric differences between model 1 and model 2 (see tables I and II) such as differences in volume, wing aspect ratio, taper, sweep, airfoil, twist, and size of engine pack relative to wing area; therefore, only an overall comparison of results for these two models can be made. The general level of maximum lift-drag ratios obtained at high subsonic speeds for both model 1 and model 2 appears rather low (between 7.25 and 8.15) when compared with efficient subsonic configurations; however, these models represented configurations designed to cruise at a Mach number of 3 and they had relatively high lift-drag ratios for the design condition (refs. 1 and 2).

L
8
8
7

Lateral Characteristics

The static directional stability of model 1 as obtained from tests of the model at $\beta = \pm 4^{\circ}$ (fig. 12) was adequate at low angles of attack and became very high as the angle of attack increased to 24°. This increase in C_{n_β} was caused by both an increase in the vertical-tail contribution (fig. 15) and by the wing-fuselage configuration becoming highly directionally stable at high angles of attack (fig. 12). Because the directional stability of model 1 was so high both at subsonic speeds (fig. 12) and at supersonic speeds (ref. 1), the relative size of the vertical tail surfaces was decreased in the design of model 2. Values of C_{n_β} obtained for model 2 were less than those for model 1; however, the static directional stability of model 2 was good at low angles of attack and increased at high angles (fig. 20).

The effective dihedral of both models was positive $\left(-C_{l_\beta}\right)$ for positive lifting conditions and became high in most cases at high angles of attack. These large values of effective dihedral may not be desirable from the standpoint of dynamic lateral characteristics; however, the use

of negative geometric dihedral in the wing of model 1 appeared satisfactory at supersonic speeds where zero effective dihedral was obtained near a reasonable cruise lift coefficient (refs. 1 and 6).

Langley Research Center,
National Aeronautics and Space Administration,
Langley Field, Va., March 11, 1960.

L
8
8
7

REFERENCES

1. Church, James D., Hayes, William C., Jr., and Sleeman, William C., Jr.: Investigation of Aerodynamic Characteristics of an Airplane Configuration Having Tail Surfaces Outboard of the Wing Tips at Mach Numbers of 2.30, 2.97, and 3.51. NACA RM L58C25, 1958.

2. Sleeman, William C., Jr., Church, James D., and Fournier, Roger H.: Aerodynamic Characteristics of a 60° Sweptback-Wing Airplane Configuration Having Tail Surfaces Located Outboard of the Wingtips at Mach Numbers of 2.30, 2.97, 3.51, and 4.06. NASA TM X-219, 1960.

3. Driver, Cornelius, and Spearman, M. Leroy: Static Stability and Control Characteristics of an Airplane Model With Tail Surfaces Outboard of the Wing Tips at a Mach Number of 2.01. NASA TM X-47, 1959.

4. Hayes, William C., Jr., and Sleeman, William C., Jr.: Low-Speed Investigation of the Effects of Horizontal-Tail Area and Wing Sweep on the Static Longitudinal Stability and Control Characteristics of an Airplane Configuration Having Tail Surfaces Outboard of the Wing Tips. NASA MEMO 6-11-59L, 1959.

5. Sherman, Windsor L.: A Theoretical Investigation of the Dynamic Lateral Stability of Three Possible Airplane Configurations for Flight at a Mach Number of 3.0. NASA MEMO 5-15-59L, 1959.

[redacted]

TABLE I.- GEOMETRIC CHARACTERISTICS OF MODEL 1

Wing plus horizontal tail (used in reduction of data):	
Area, sq ft	1.7391
Span, ft	2.0000
Mean aerodynamic chord, ft	1.0790
Aspect ratio	2.3000
Taper ratio	0.1271
Wing:	
Area, sq ft	1.3611
Span, ft	1.1667
Mean aerodynamic chord, ft	1.2409
Aspect ratio	1.0000
Taper ratio	0.3919
Airfoil section	NACA 65A004
Twist, deg:	
Root	0
Tip	-2.8
Dihedral, deg	-5.3
Leading-edge sweepback, deg	70.0
Exposed volume, cu ft	0.0295
Horizontal or vertical tail surface (panel geometry):	
Area, sq ft	0.1890
Span, ft	0.4167
Mean aerodynamic chord, ft	0.4962
Aspect ratio	0.9185
Taper ratio	0.3069
Airfoil section	NACA 65A003
Twist, deg	0
Dihedral, deg	0
Leading-edge sweepback, deg	60.0
Exposed volume, cu ft	0.0013
Fuselage:	
Length, ft	2.8057
Fineness ratio	12.5
Volume, cu ft	0.0694
Wingtip body:	
Length, ft	2.0833
Fineness ratio	16.6667
Volume, cu ft	0.0169
Engine pack:	
Base area (excluding the three exits), sq ft	0.0178
Enclosed volume, cu ft	0.0181
Volume parameter (excluding engine pack), $\frac{(\text{Volume})^{2/3}}{S}$	0.154

[redacted]

TABLE II.- GEOMETRIC CHARACTERISTICS OF MODEL 2

Wing plus horizontal tail (used in reduction of all data):	
Area, sq ft	2.5000
Span, ft	2.2941
Mean aerodynamic chord, ft	1.3690
Aspect ratio	2.1052
Taper ratio	0.0986
Wing:	
Area, sq ft	2.0833
Span, ft	1.3693
Mean aerodynamic chord, ft	1.5419
Aspect ratio	0.9000
Taper ratio	0.6654
Twist, deg	0
Dihedral, deg	0
Leading-edge sweepback, deg	60.00
Trailing-edge sweepback, deg	40.00
Exposed volume, cu ft	0.04021
Airfoil section	$2\frac{1}{2}$ percent thick, hexagonal
Horizontal tail surface (panel geometry):	
Area, sq ft	0.2083
Span, ft	0.4624
Mean aerodynamic chord, ft	0.5046
Aspect ratio	1.0392
Taper ratio	0.2500
Leading-edge sweepback, deg	61.50
Trailing-edge sweepback, deg	30.88
Exposed volume, cu ft	0.00187
Airfoil section	$2\frac{1}{2}$ percent thick, hexagonal
Vertical tail surface (panel geometry):	
Area, sq ft	0.1389
Span, ft	0.3223
Mean aerodynamic chord	0.4826
Aspect ratio	0.7479
Taper ratio	0.2500
Incidence (toe-out), deg	1.50
Rudder area, sq ft	0.0463
Location of rudder hinge line, percent chord	66.67
Leading-edge sweepback, deg	52.00
Trailing-edge sweepback, deg	-13.00
Exposed volume, cu ft	0.00095
Airfoil section	$2\frac{1}{2}$ percent thick, double wedge
Fuselage:	
Length, ft	3.2917
Fineness ratio	15.65
Volume, cu ft	0.06294
Wingtip body:	
Length, ft	2.2917
Fineness ratio	20.14
Volume (each), cu ft	0.01045
Engine pack:	
Base area (excluding four exits and cavity area), sq ft	0.0228
Cavity area surrounding model sting, sq ft	0.0167
Capture area, sq ft	0.0309
Enclosed volume, cu ft	0.05941
Volume parameter (excluding engine pack), $\frac{(\text{Volume})^{2/3}}{S}$	0.103

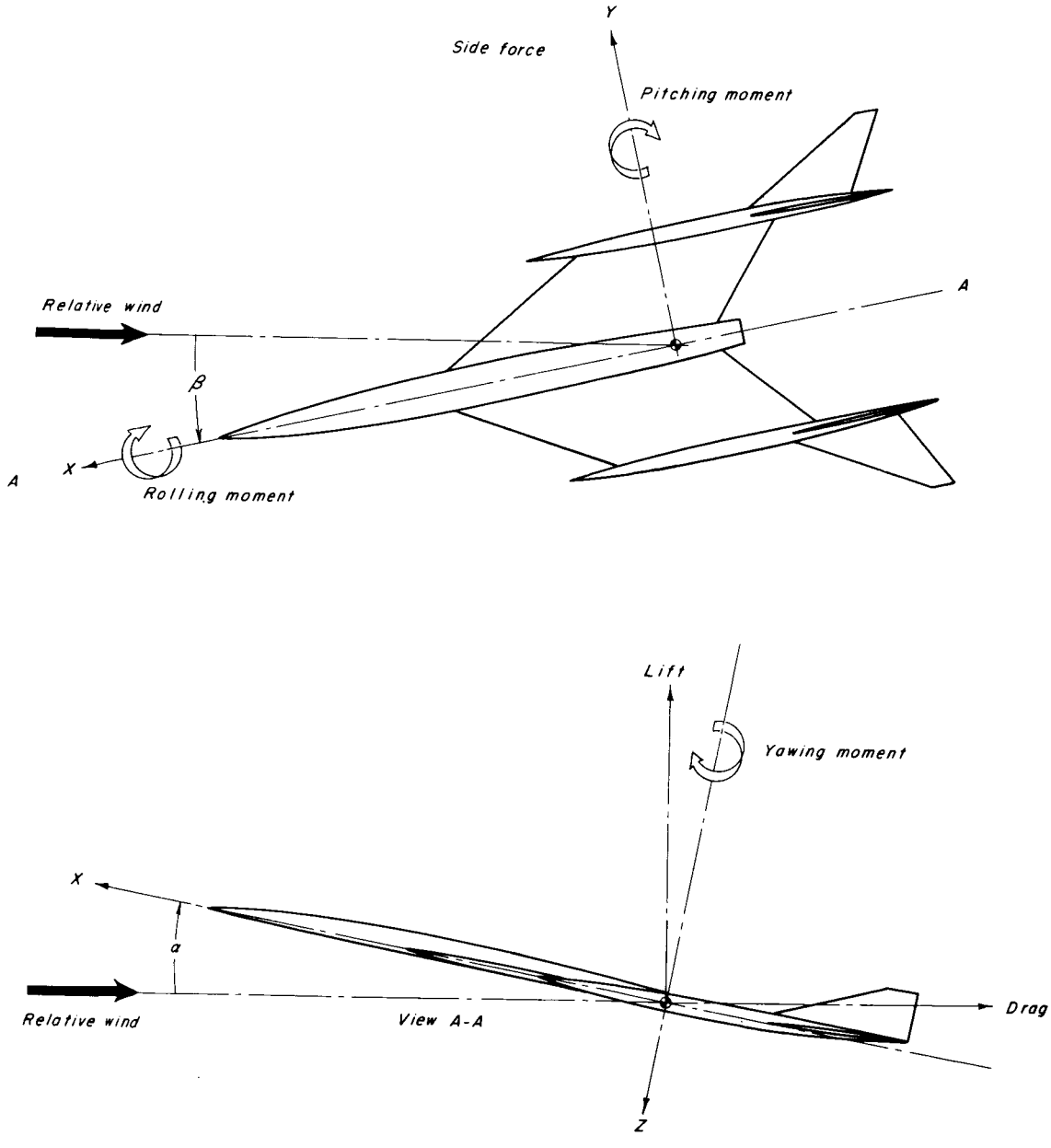

Figure 1.- System of axes used in presentation of data.

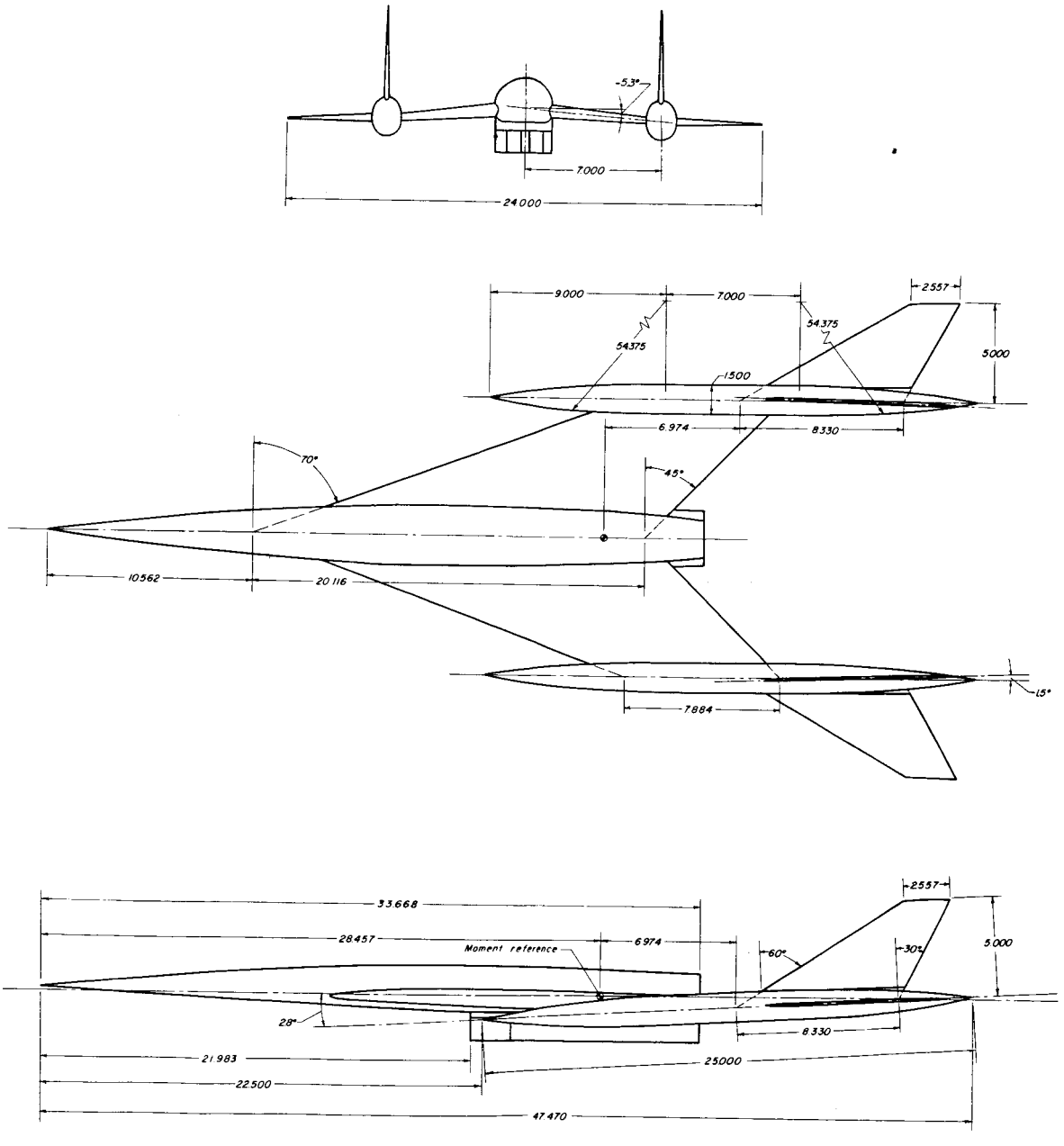

(a) Three-view drawing of model.

Figure 2.- General arrangement of model 1. All dimensions in inches.

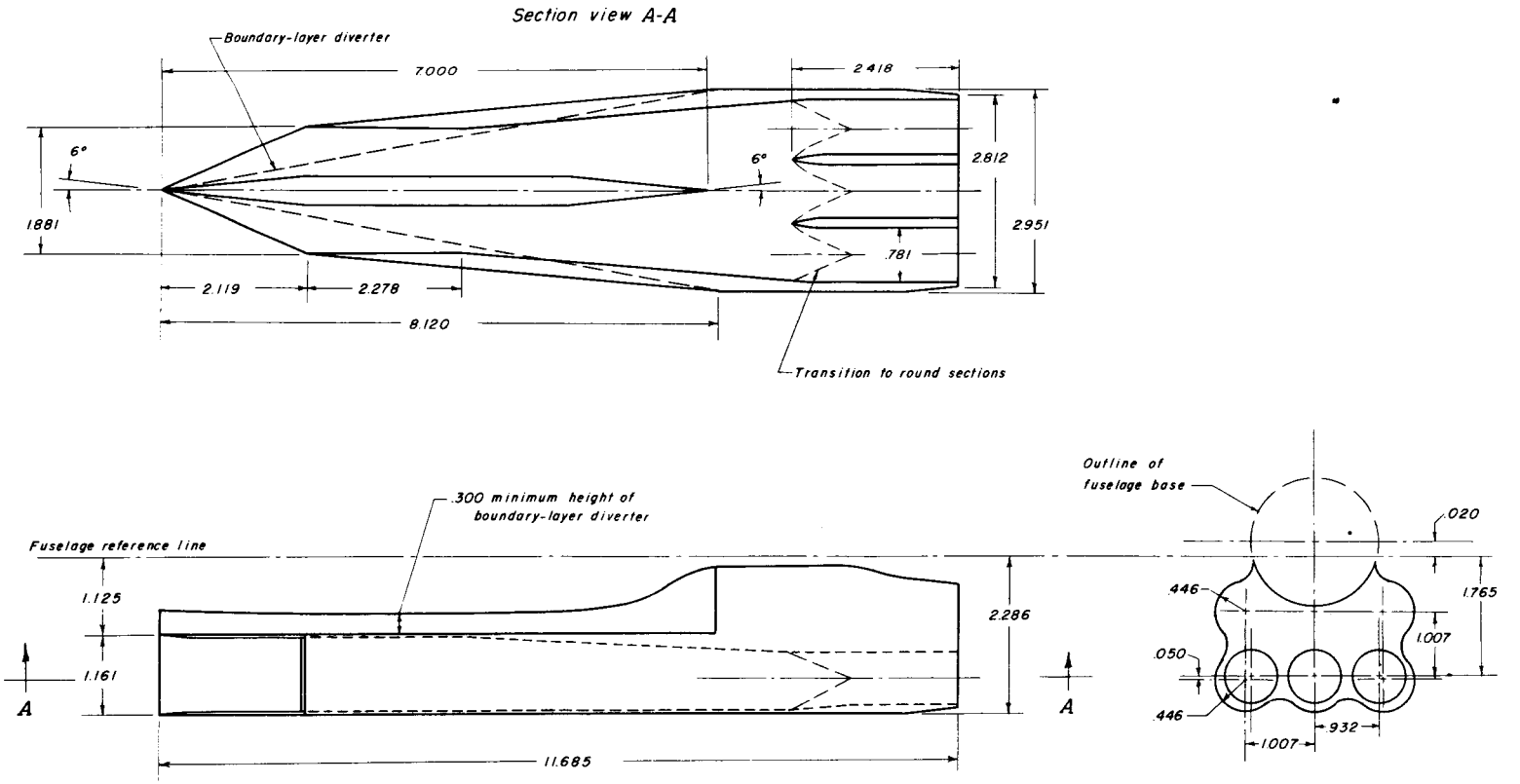

(b) Details of engine pack.

Figure 2.- Continued.

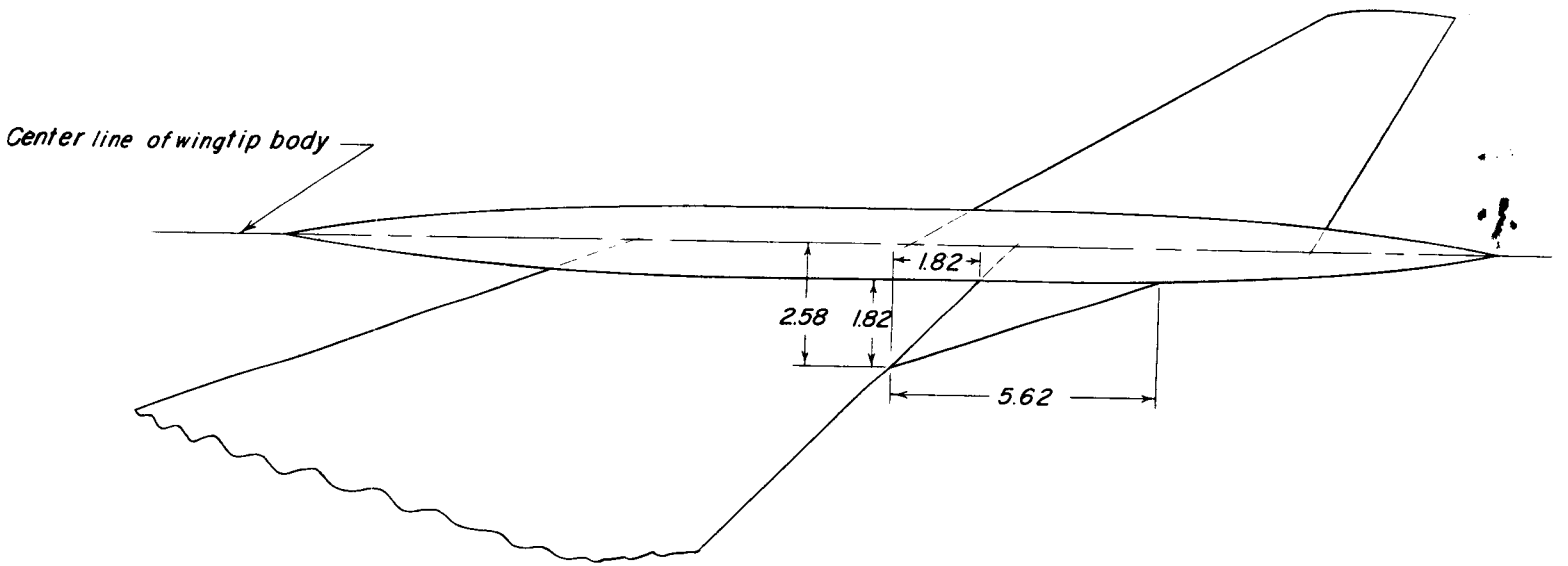

(c) Details of wing trailing-edge extension.

Figure 2.- Continued.

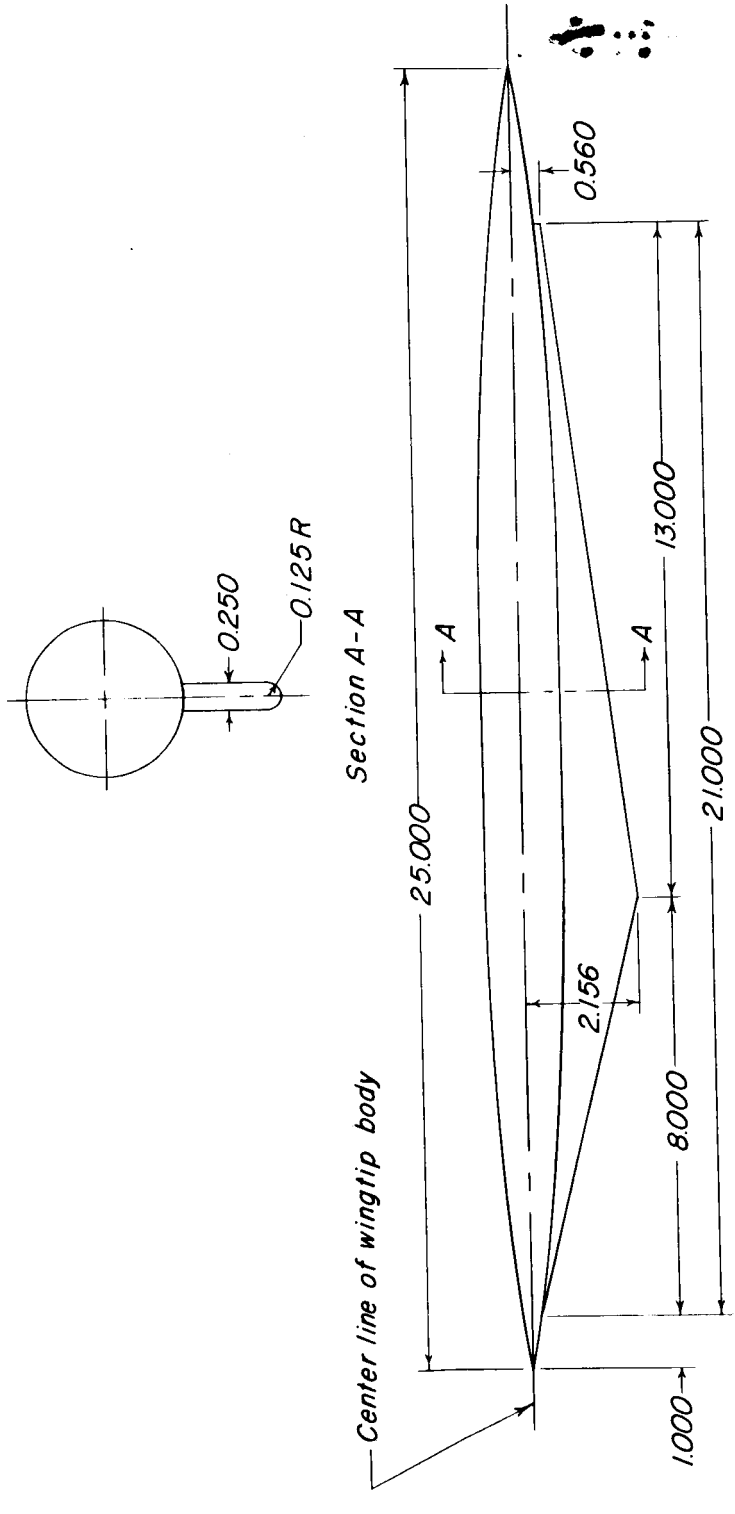

(d) Details of ventral fin mounted on wingtip body.

Figure 2.- Concluded.

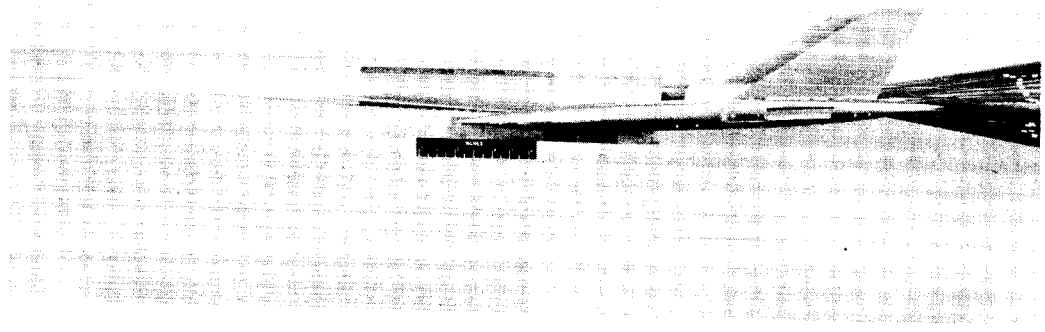

L-57-4302

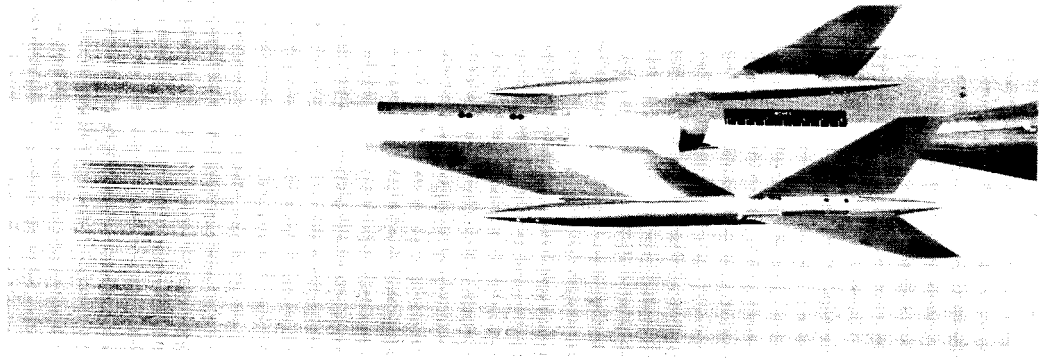

L-57-4303

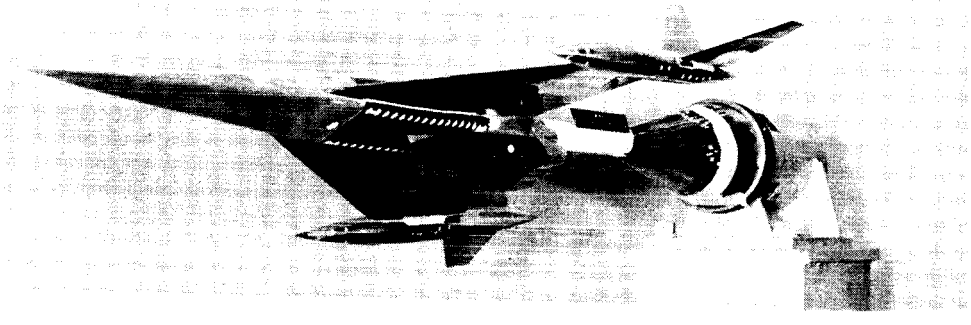

L-57-4301

Figure 3.- Photographs of model 1.

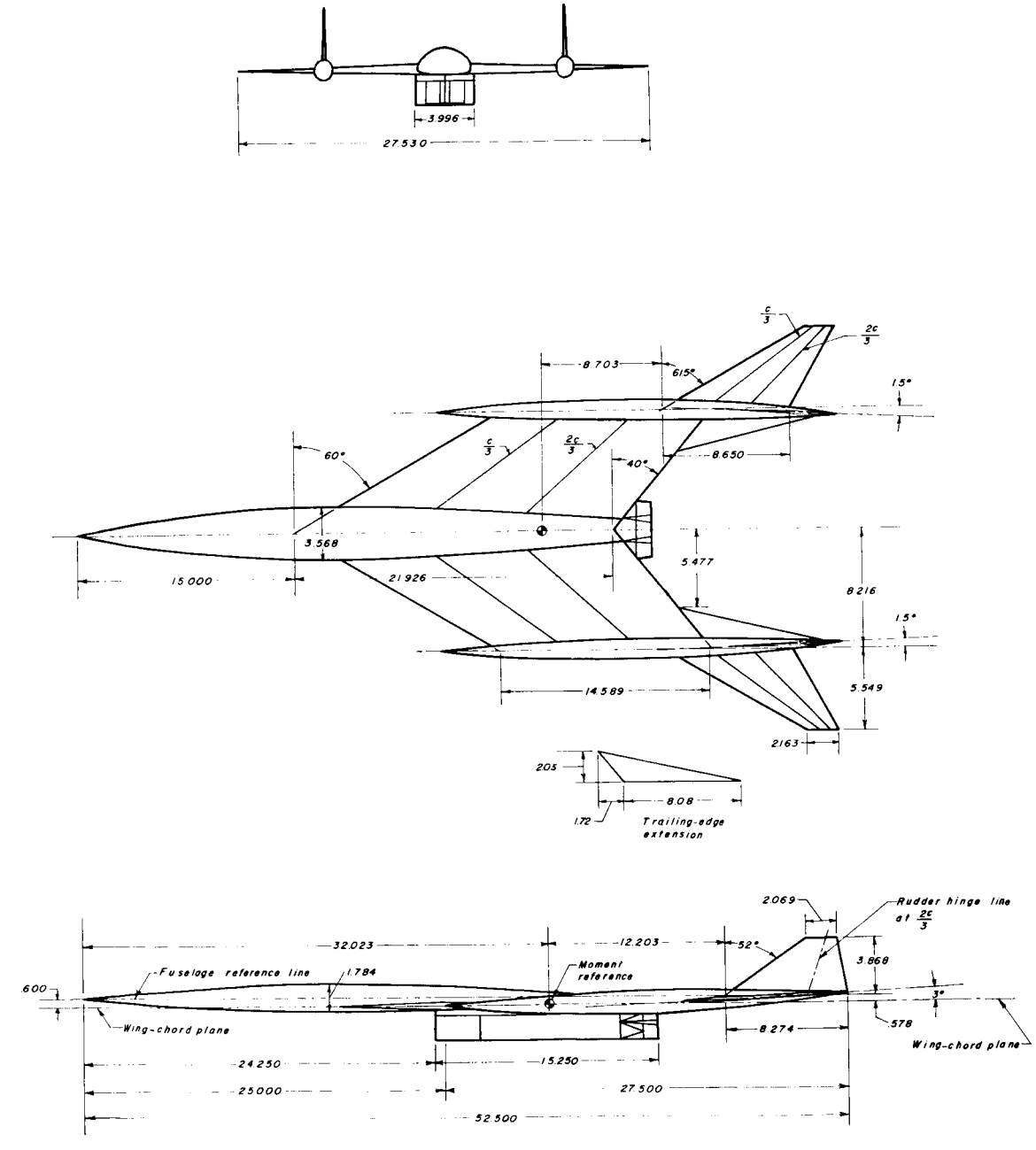

(a) Three-view drawing of model.

Figure 4.- General arrangement of model 2. All dimensions in inches.

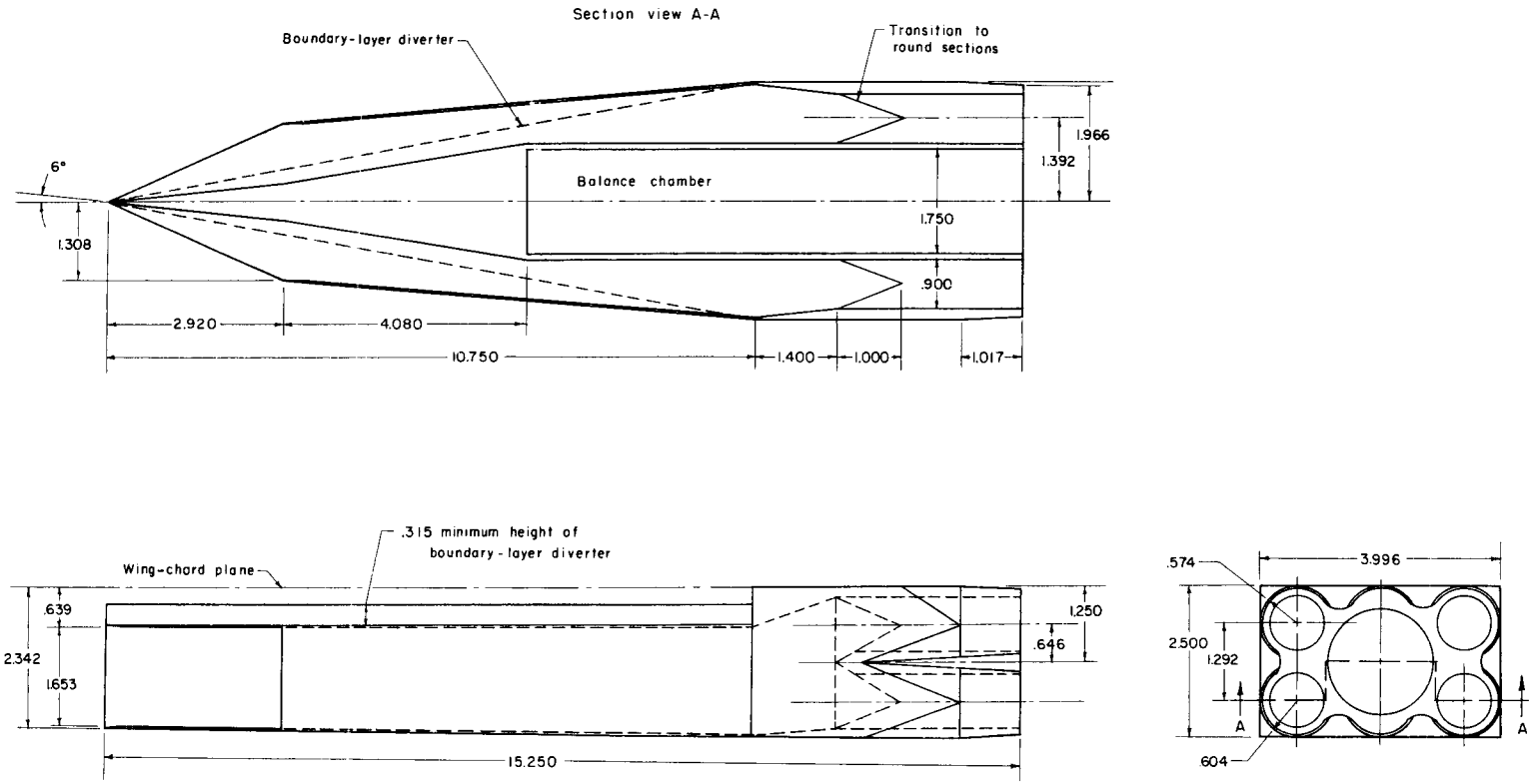

(b) Details of engine pack.

Figure 4.- Concluded.

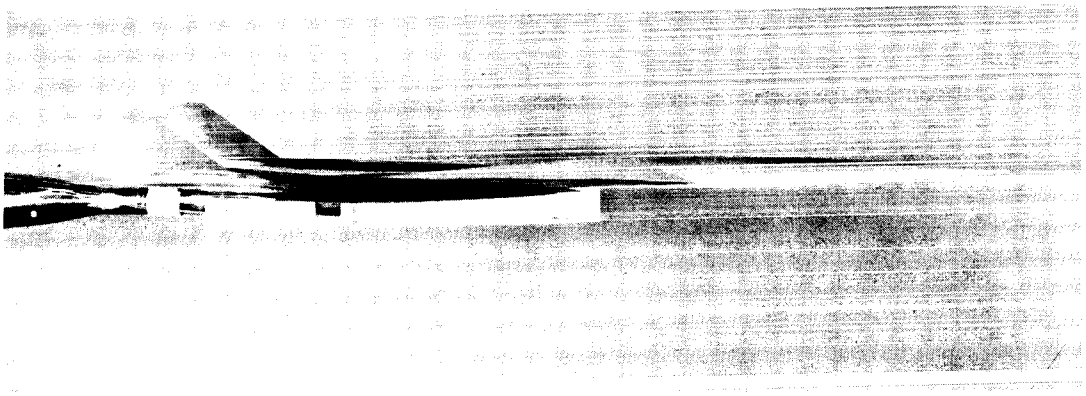

L-58-2291

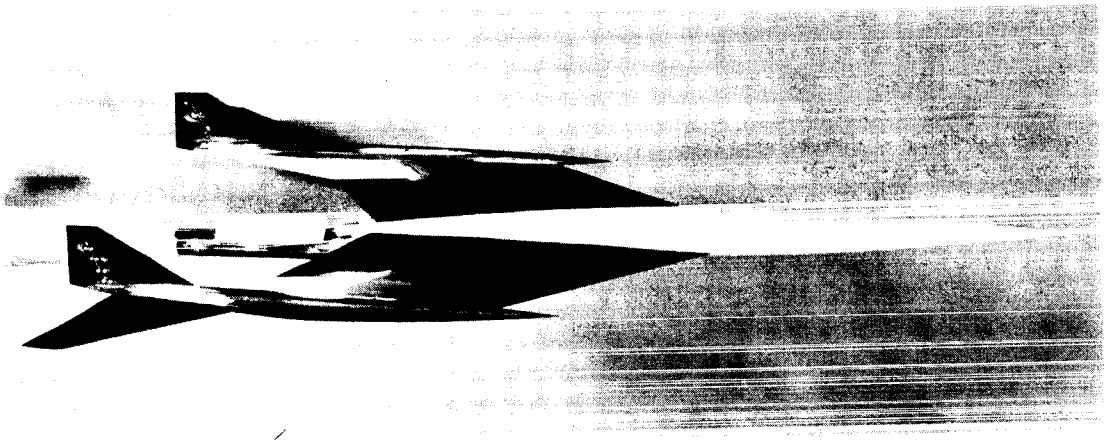

L-58-2294

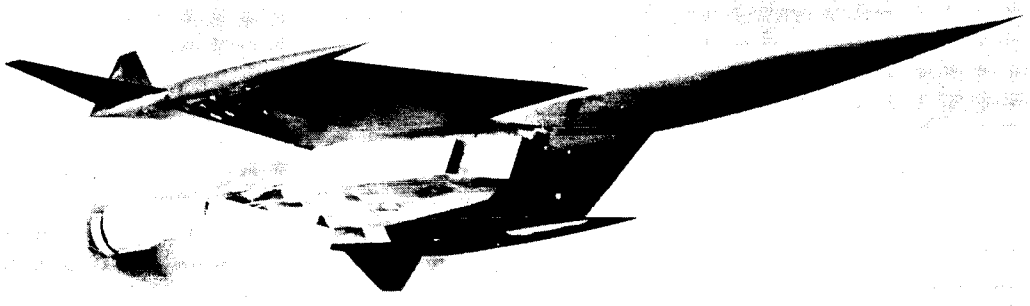

L-58-2297

Figure 5.- Photographs of model 2.

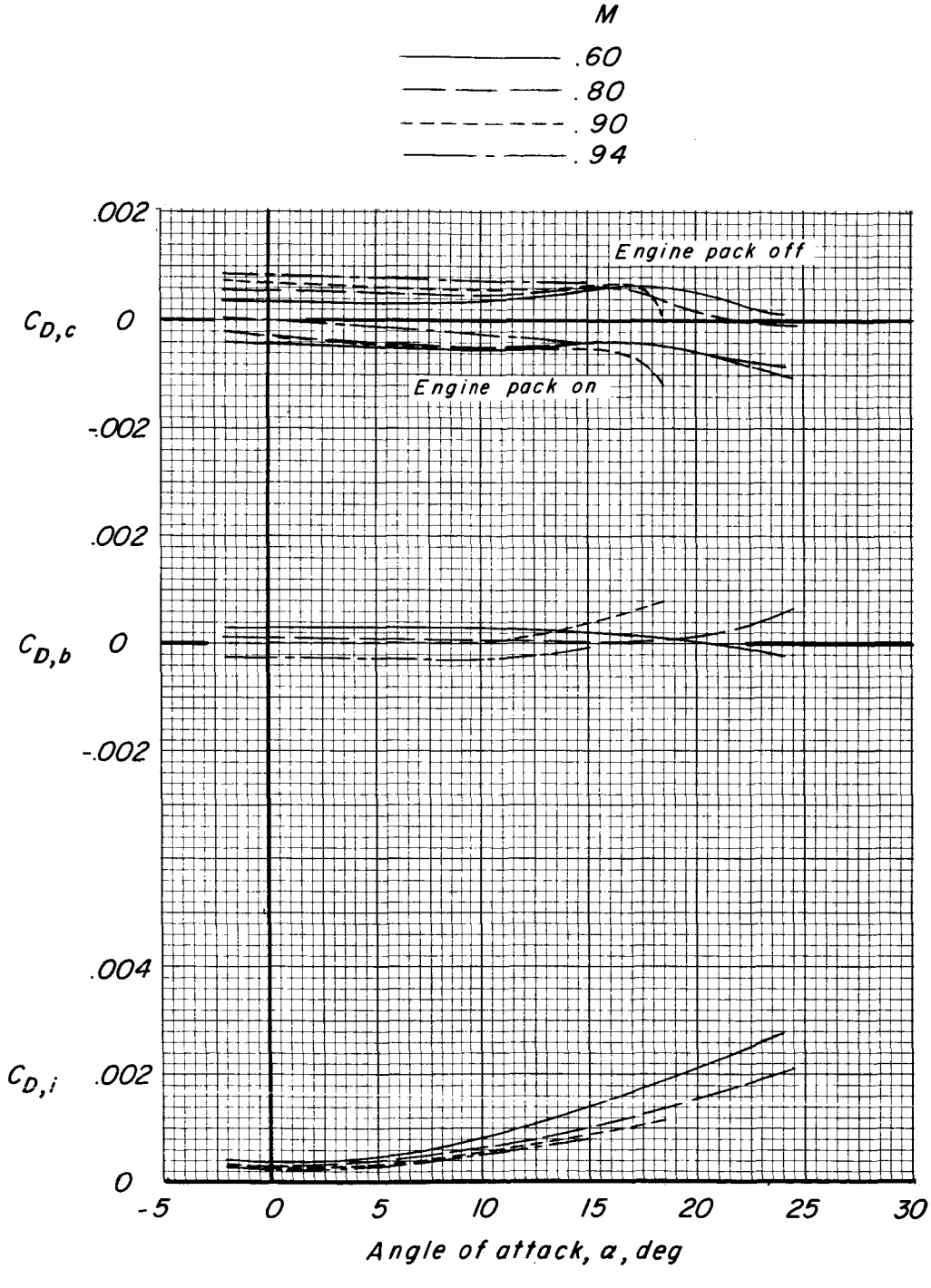

(a) Model 1.

Figure 6.- Drag corrections applied to the data.

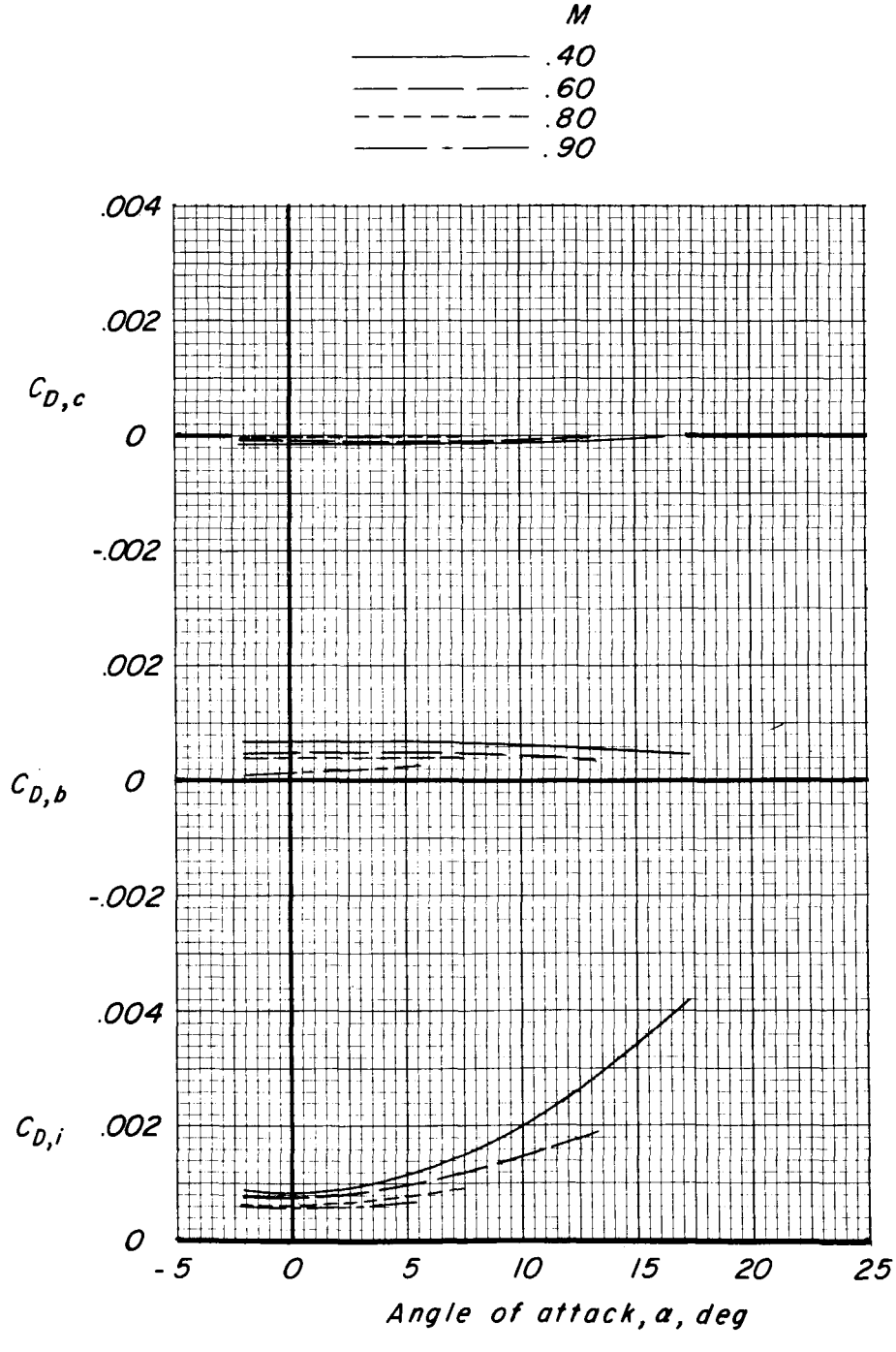

(b) Model 2.

Figure 6.- Concluded.

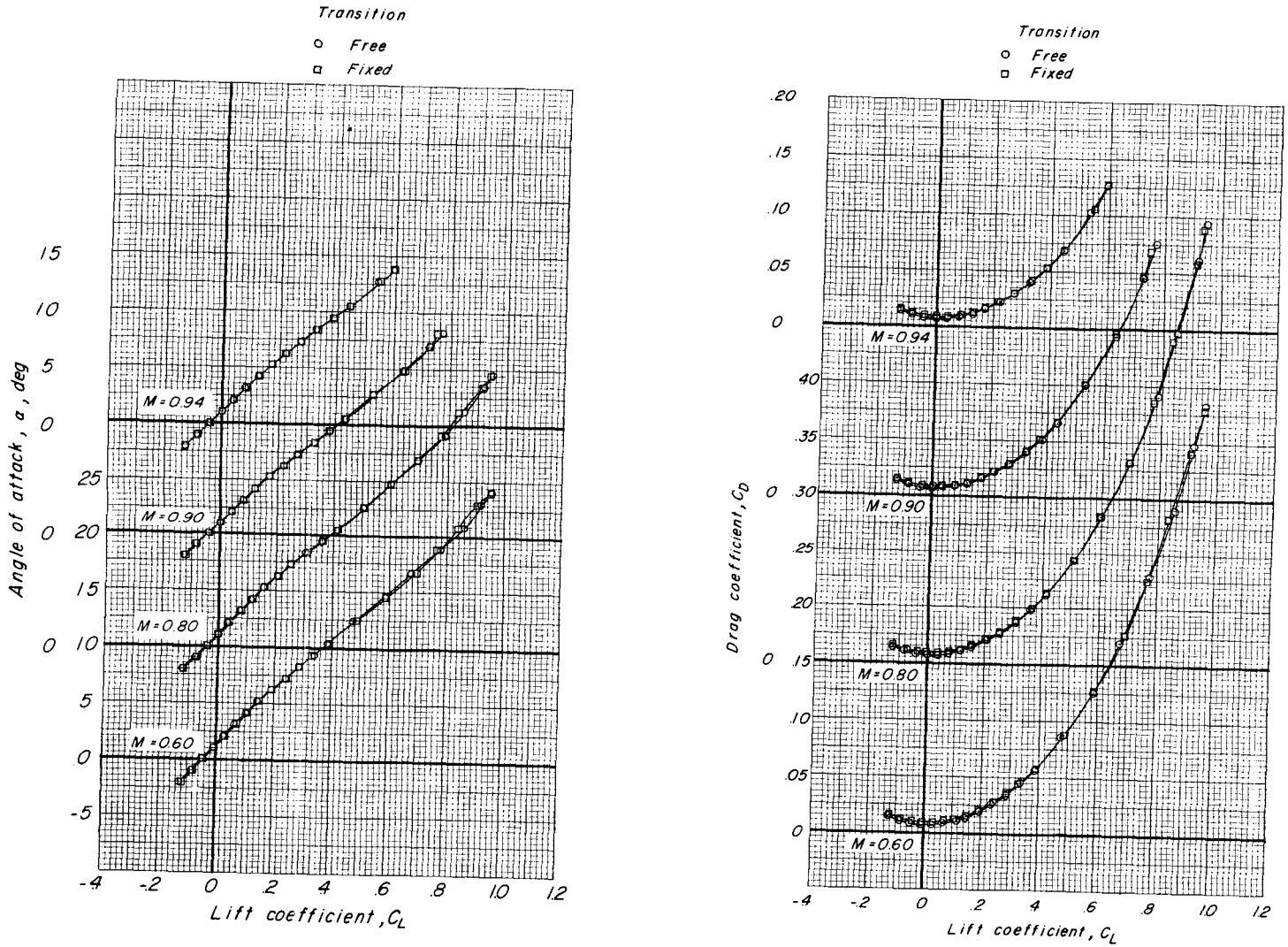

Figure 7.- Effect of fixing transition on the longitudinal characteristics of model 1 with the engine pack removed. Configuration WBOVH; $i_t = 0.1^\circ$.

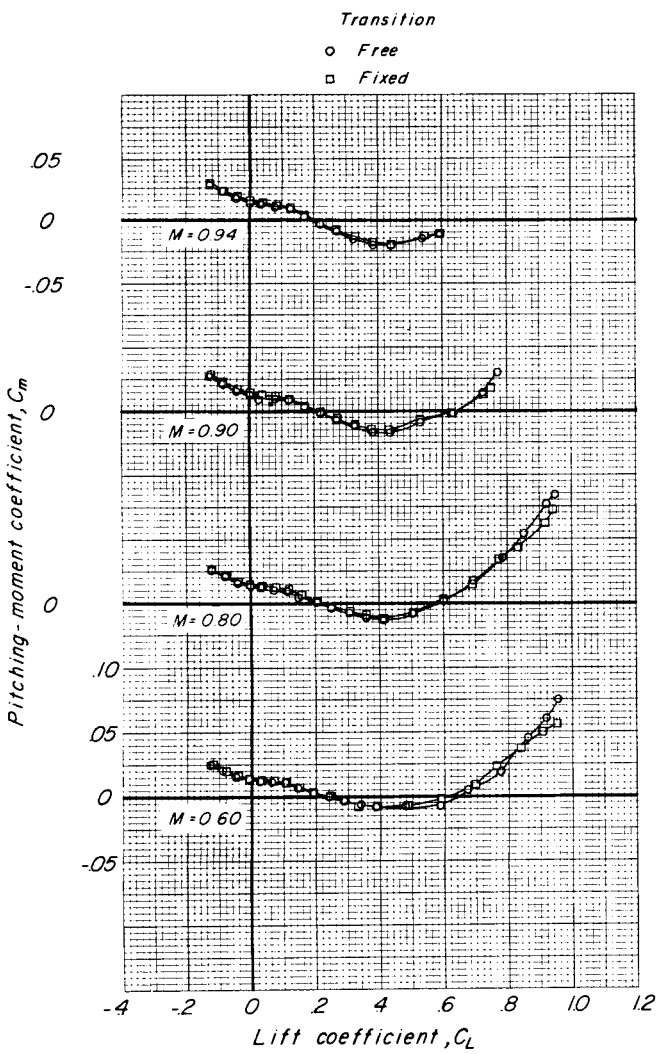

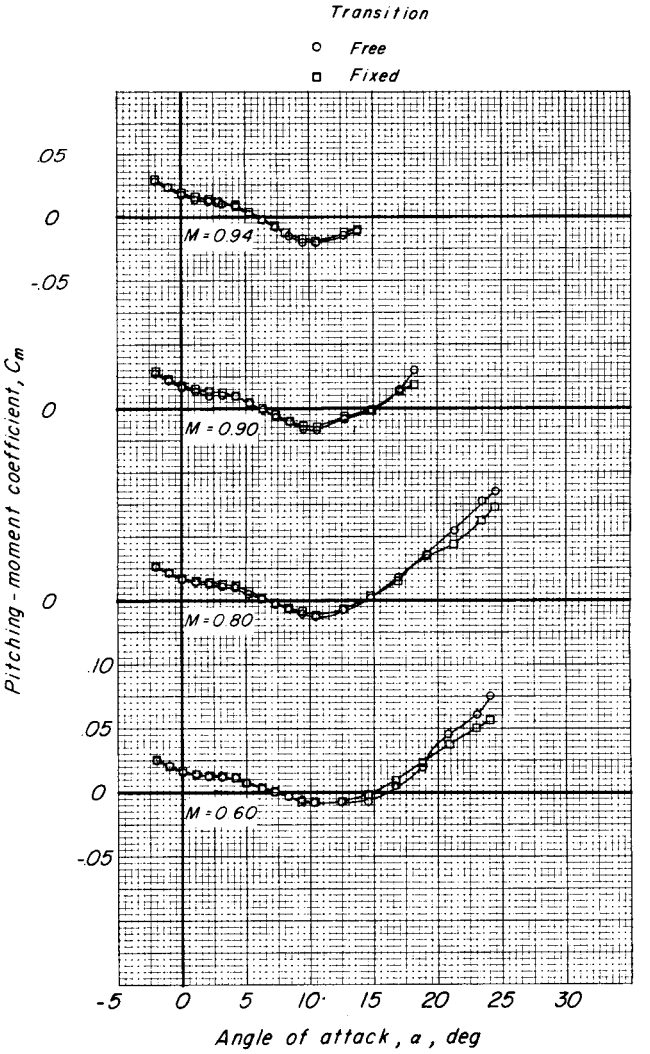

Figure 7.- Concluded.

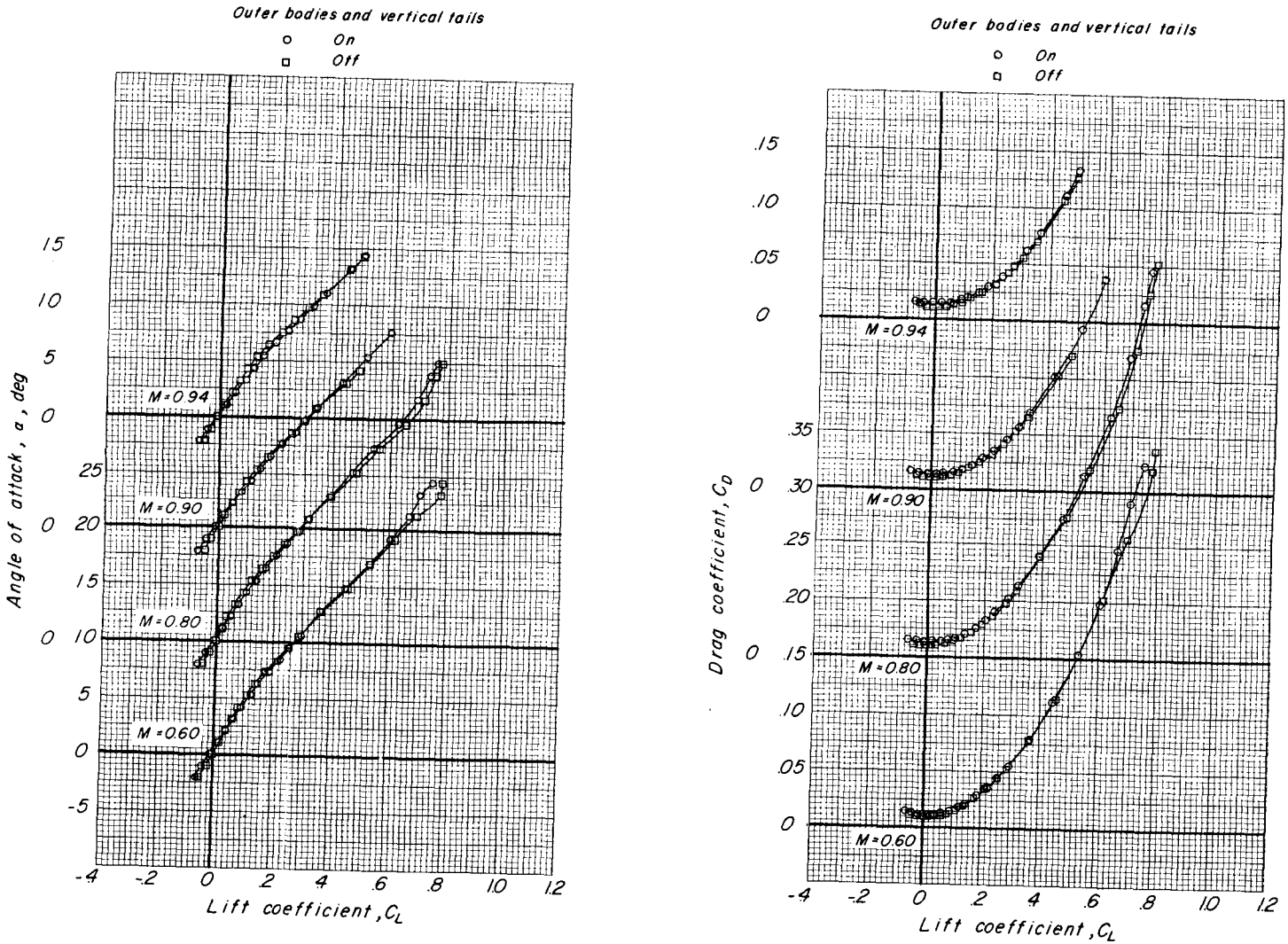

Figure 8.- Effect of vertical tails and wingtip bodies on the longitudinal characteristics of model 1 with the horizontal tail removed. Configurations WBEOV and WBE.

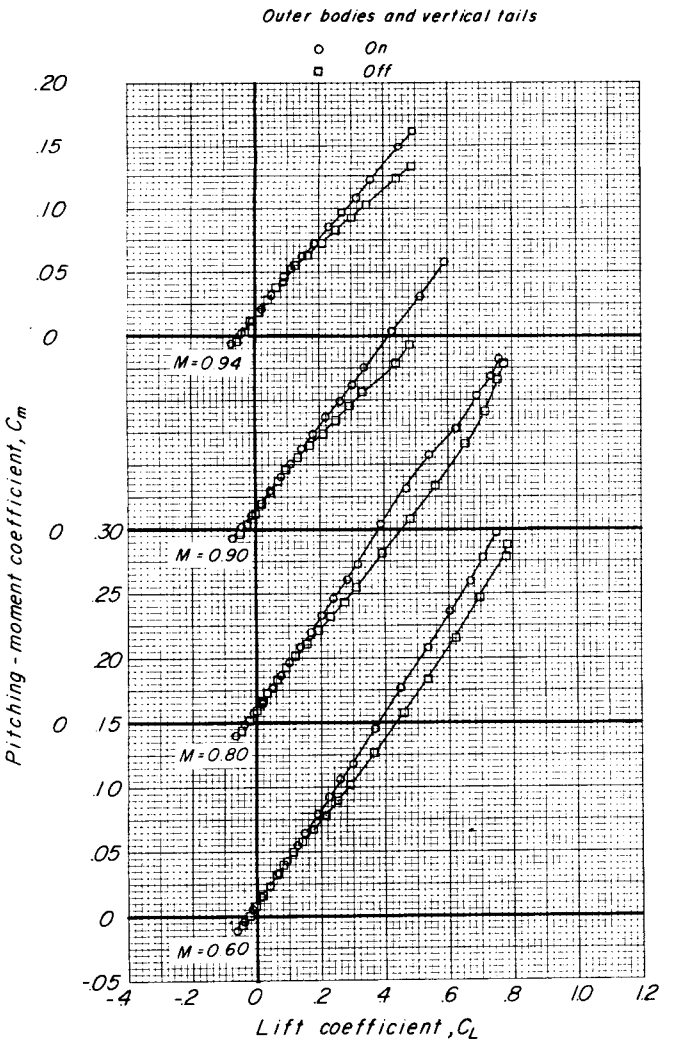

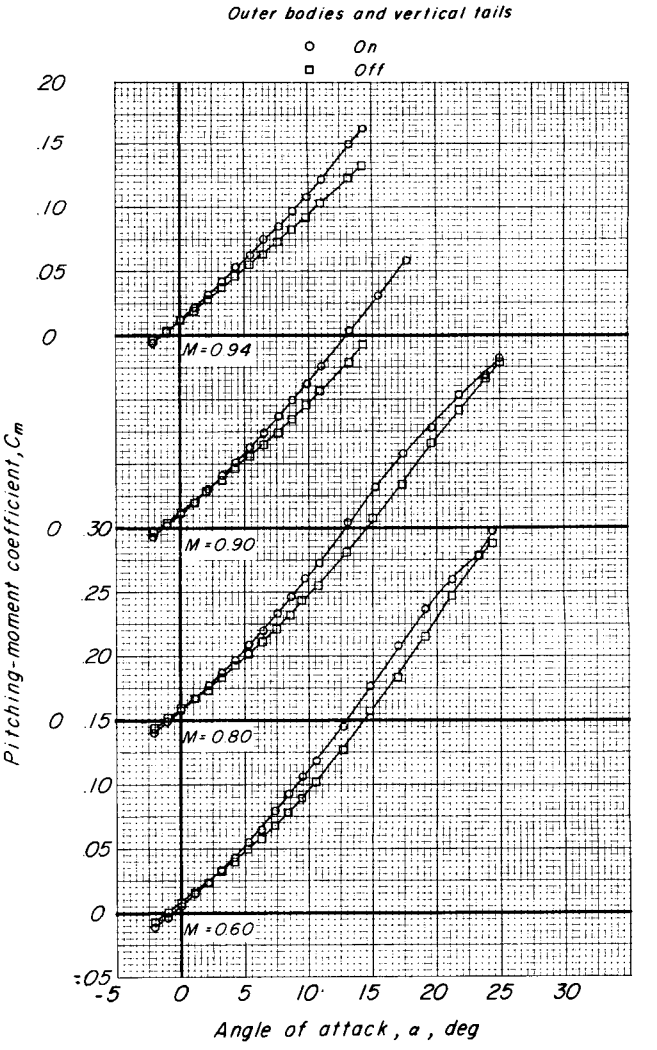

Figure 8.- Concluded.

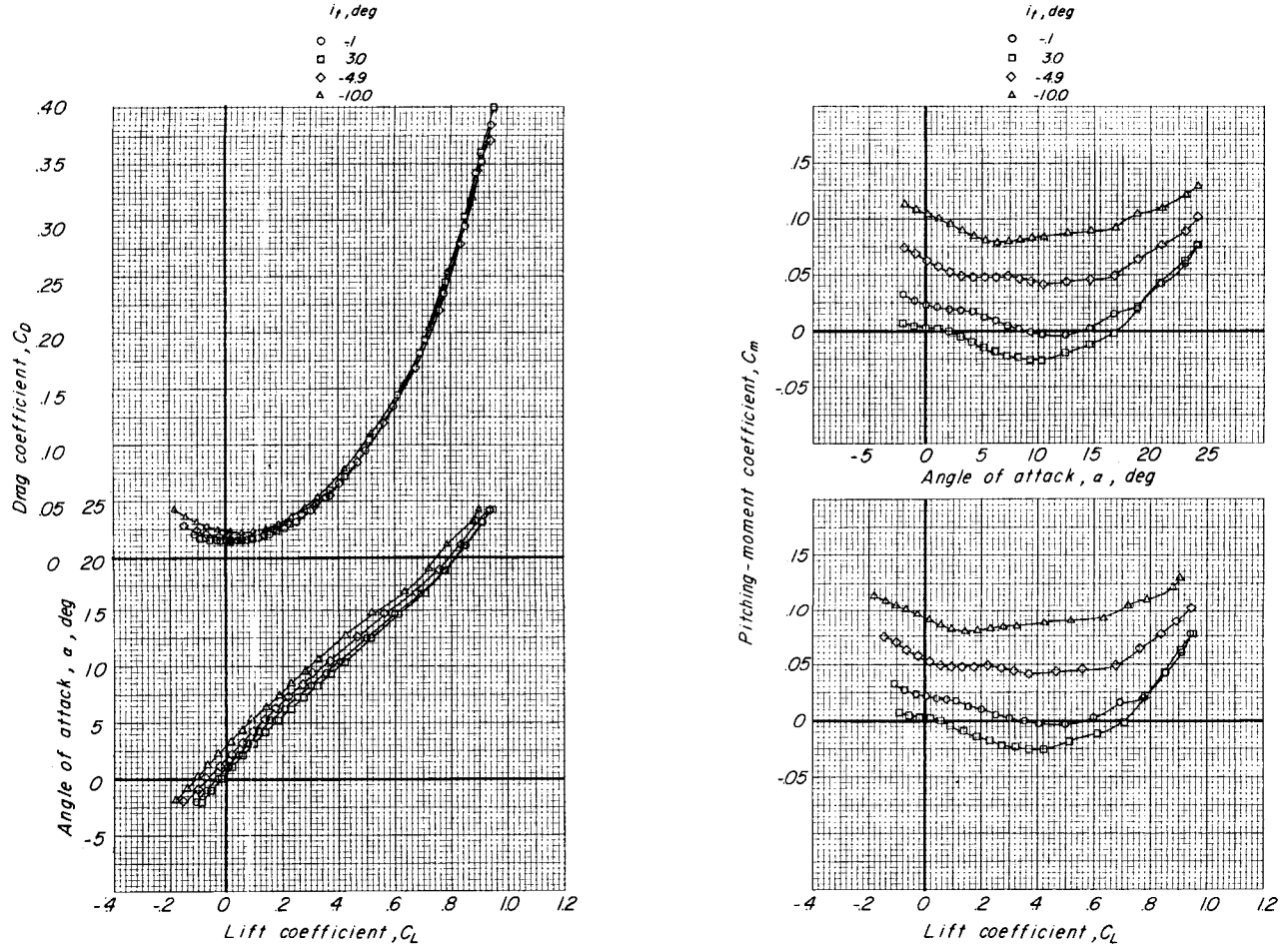

(a) M = 0.60.

Figure 9.- Effect of horizontal-tail incidence on the longitudinal characteristics of model 1. Configuration WBEOVH.

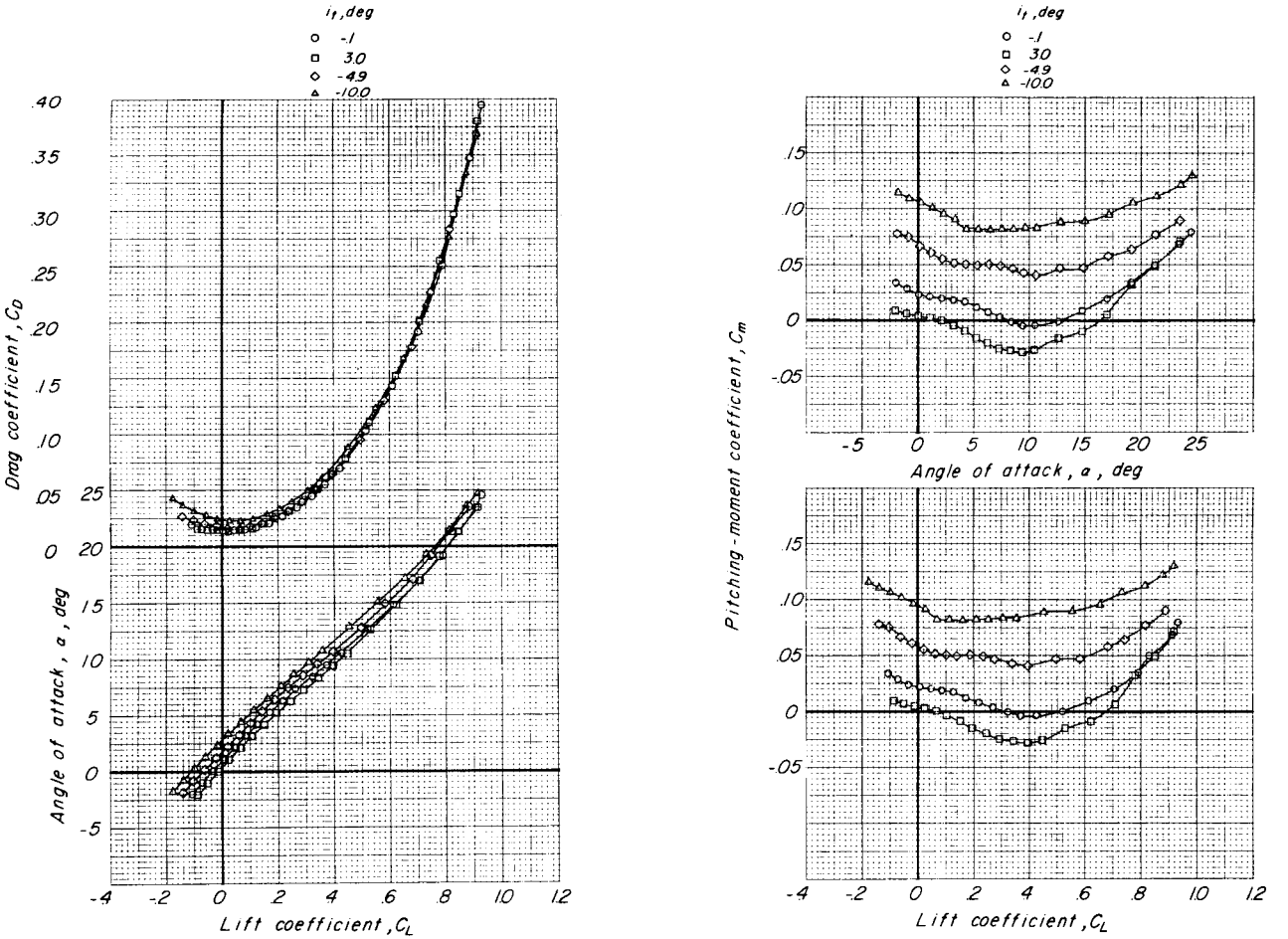

(b) M = 0.80.

Figure 9.- Continued.

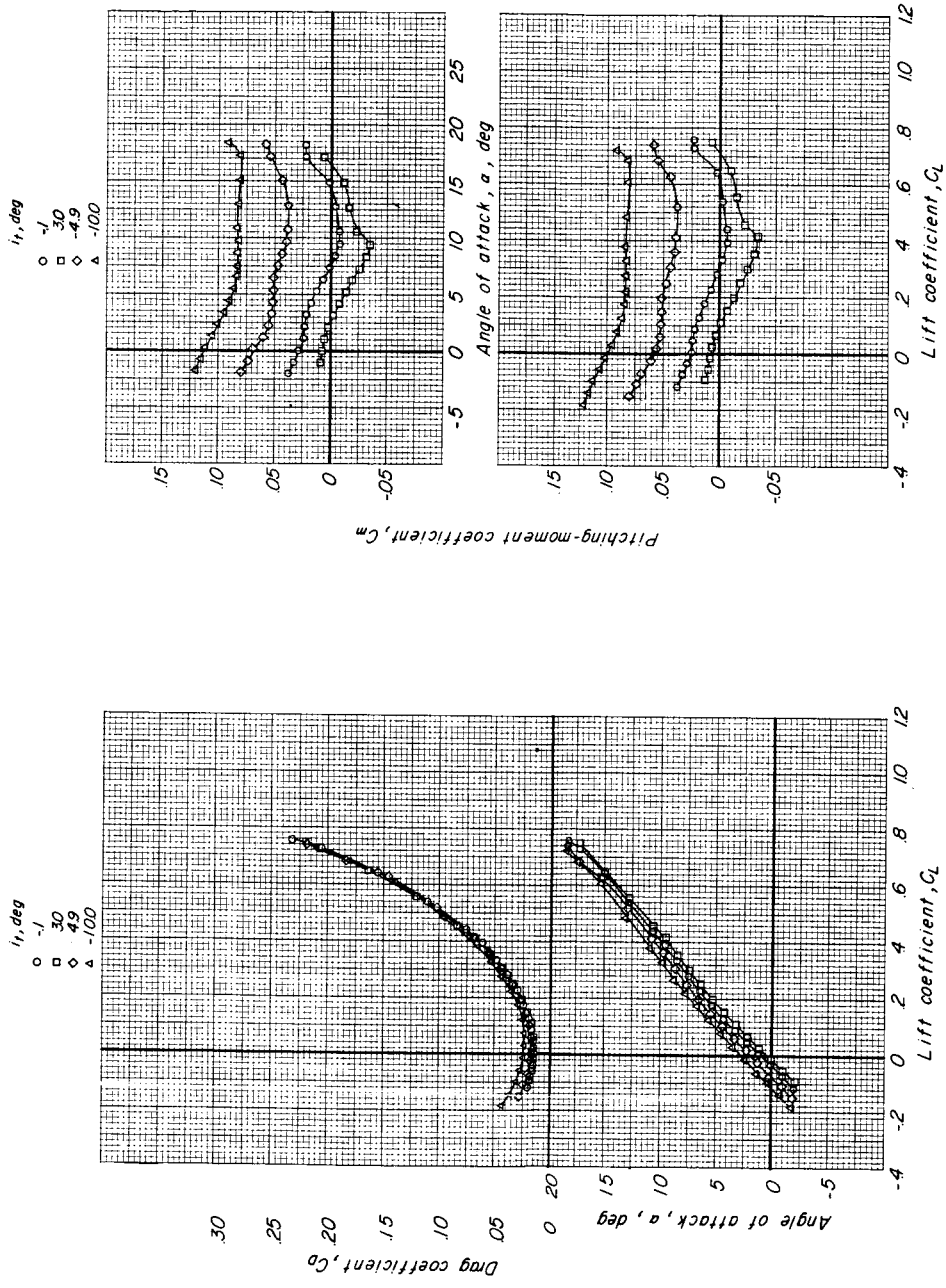

(c) M = 0.90.

Figure 9.- Continued.

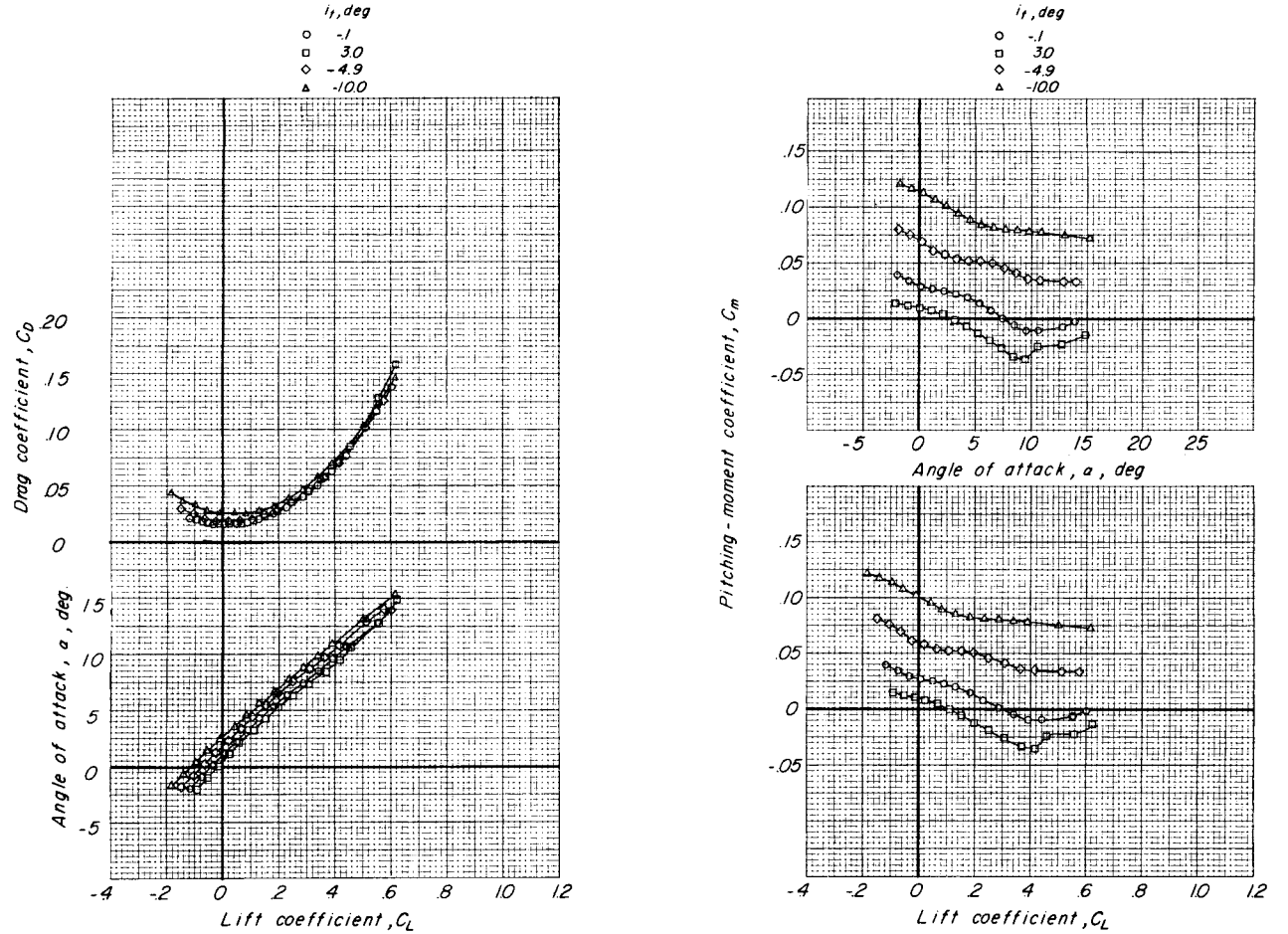

(d) M = 0.94.

Figure 9.- Concluded.

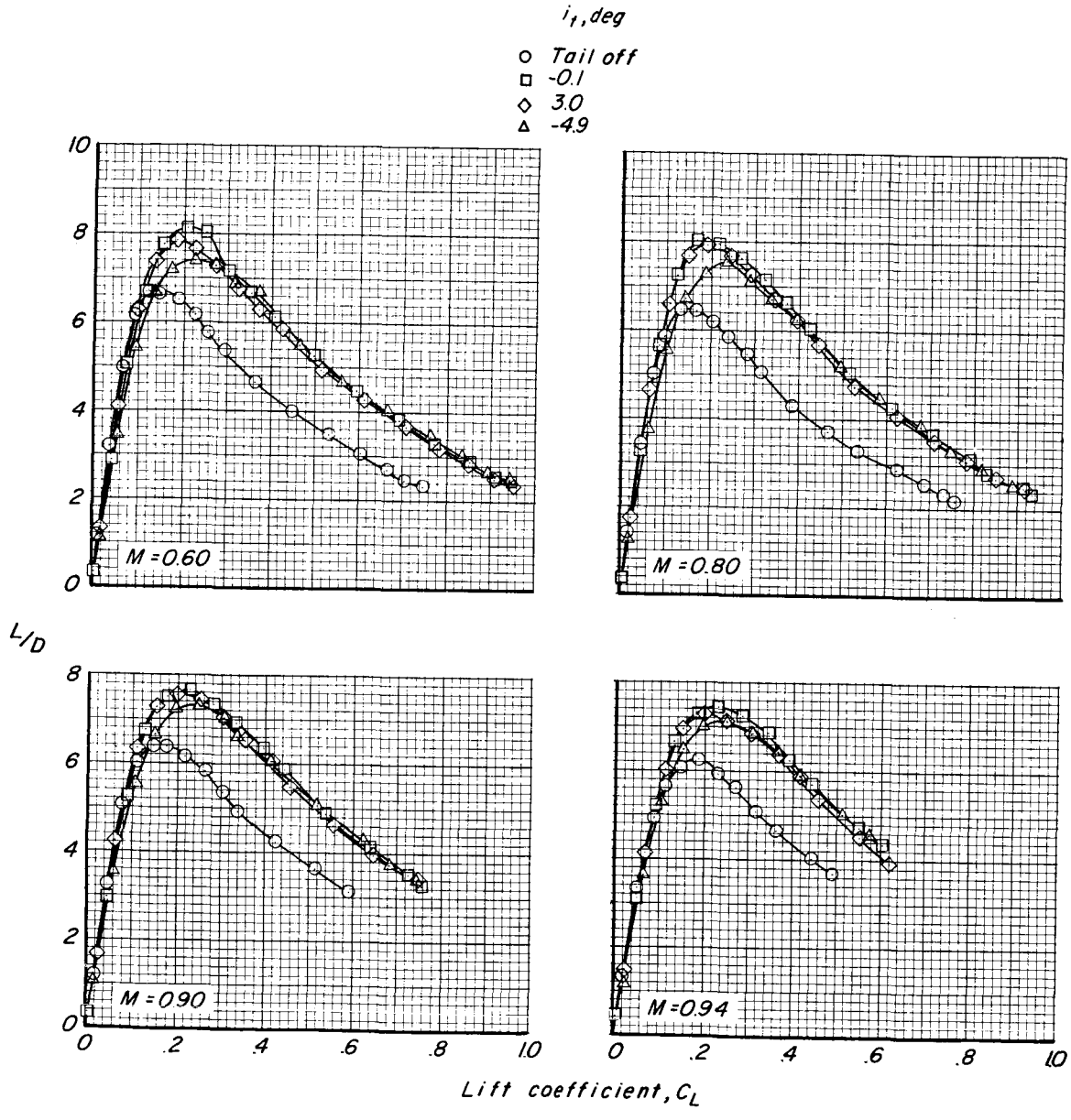

Figure 10.- Effect of horizontal-tail incidence on lift-drag ratios of model 1. Configuration WBEOVH.

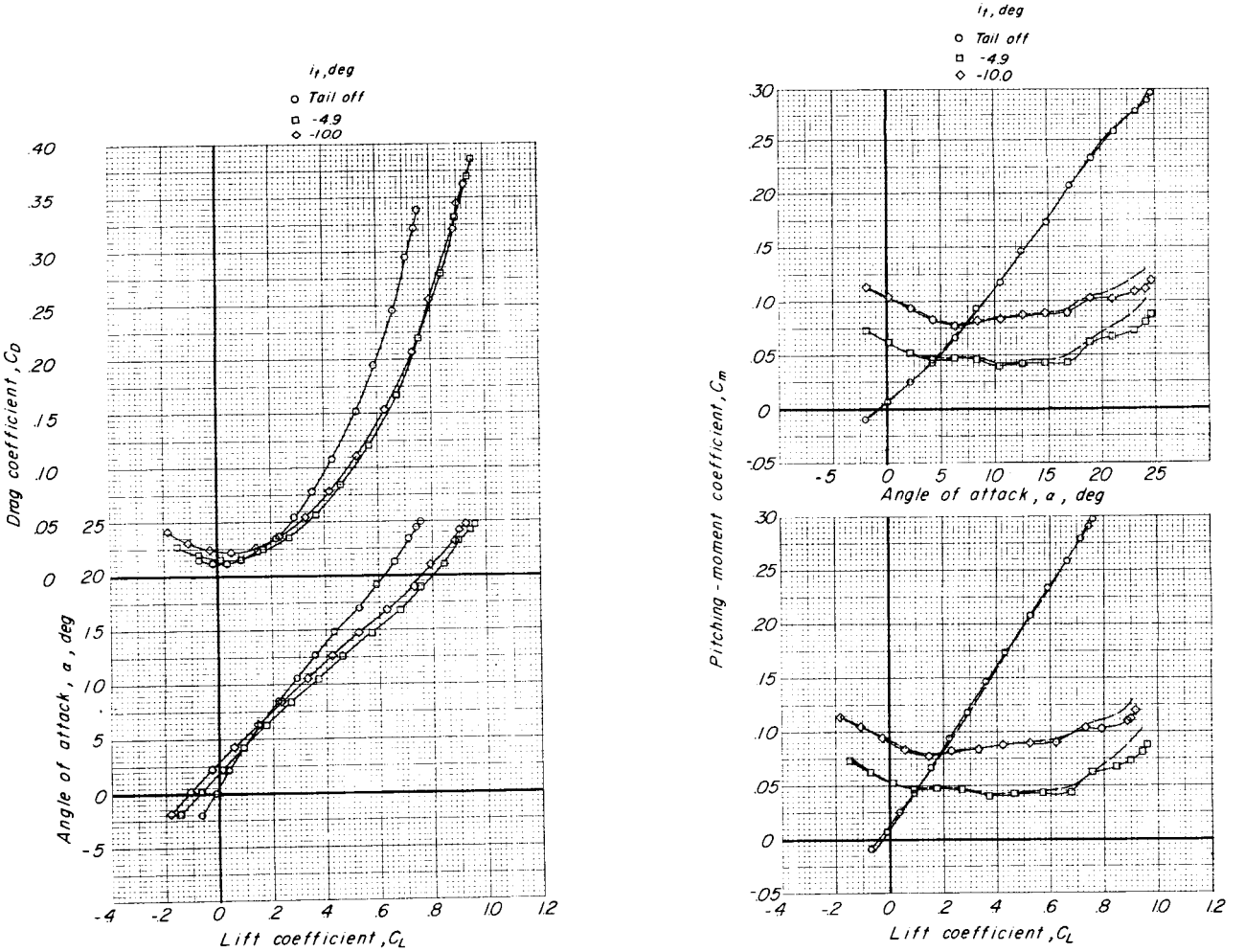

Figure 11.- Longitudinal characteristics of model 1 with the wing trailing-edge extension on. M = 0.60; configuration WBEOVH + Extension. (Pitching-moment coefficients for basic model indicated by dashed lines.)

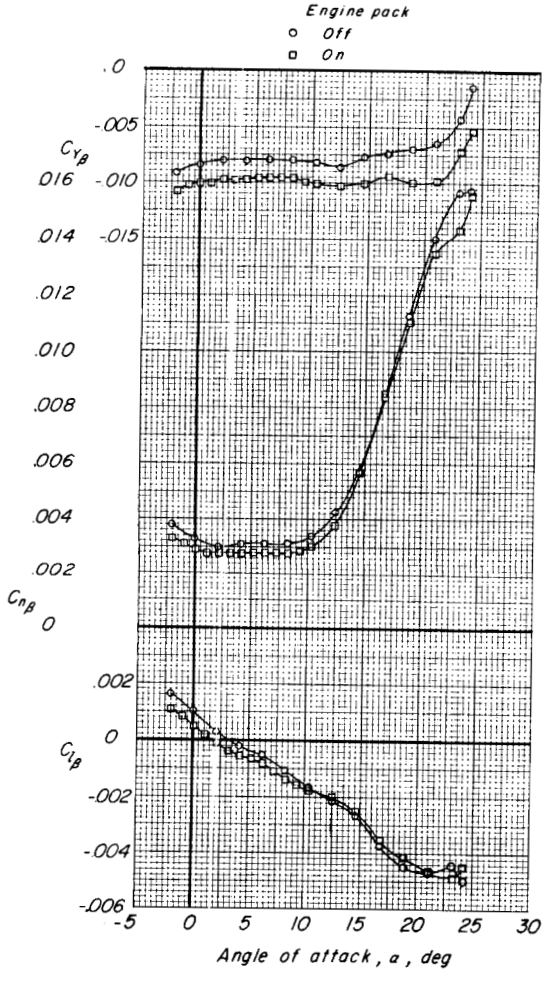

(a) M = 0.60.

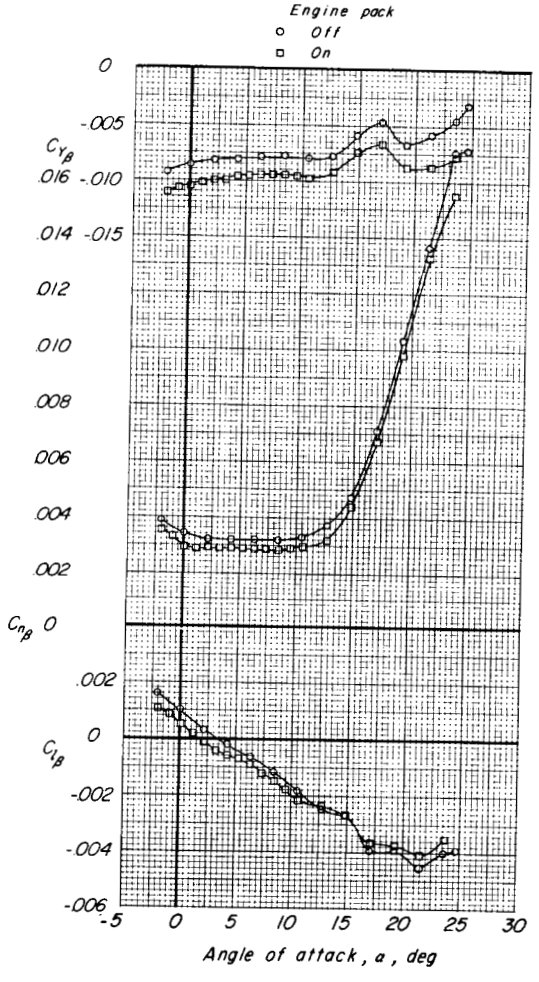

(b) M = 0.80.

Figure 12.- Effect of engine pack on the static lateral-stability derivatives of model 1. Configurations WBEOVH and WBOVH; $i_t = -0.1^\circ$.

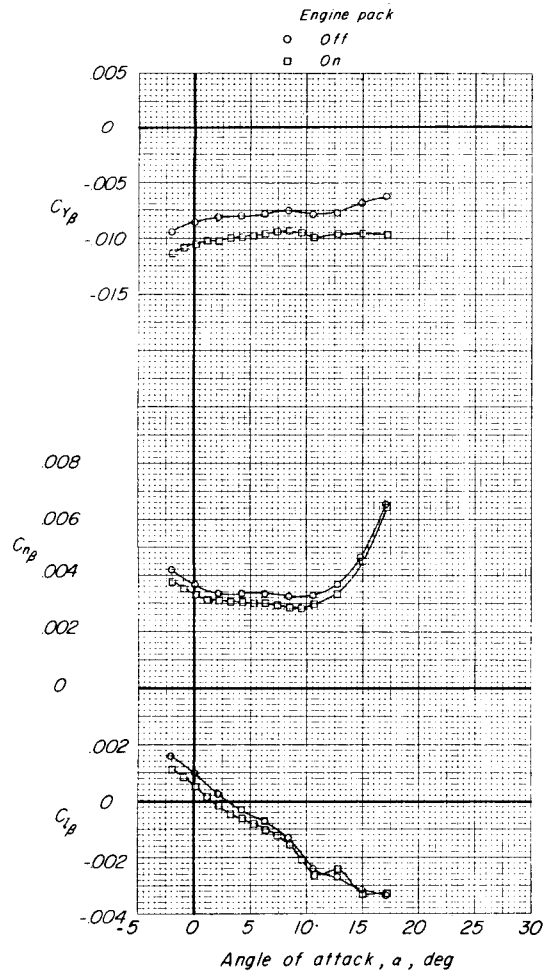

(c) M = 0.90.

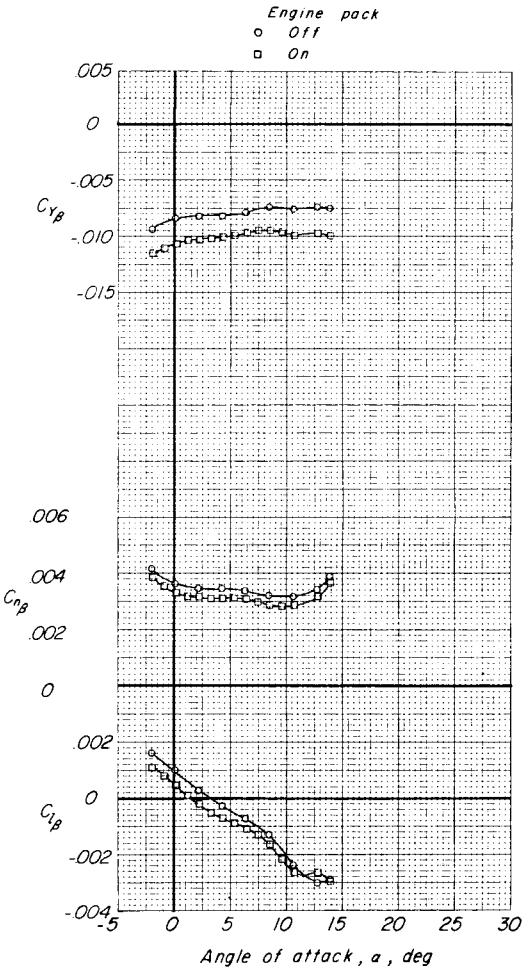

(d) M = 0.94.

Figure 12.- Concluded.

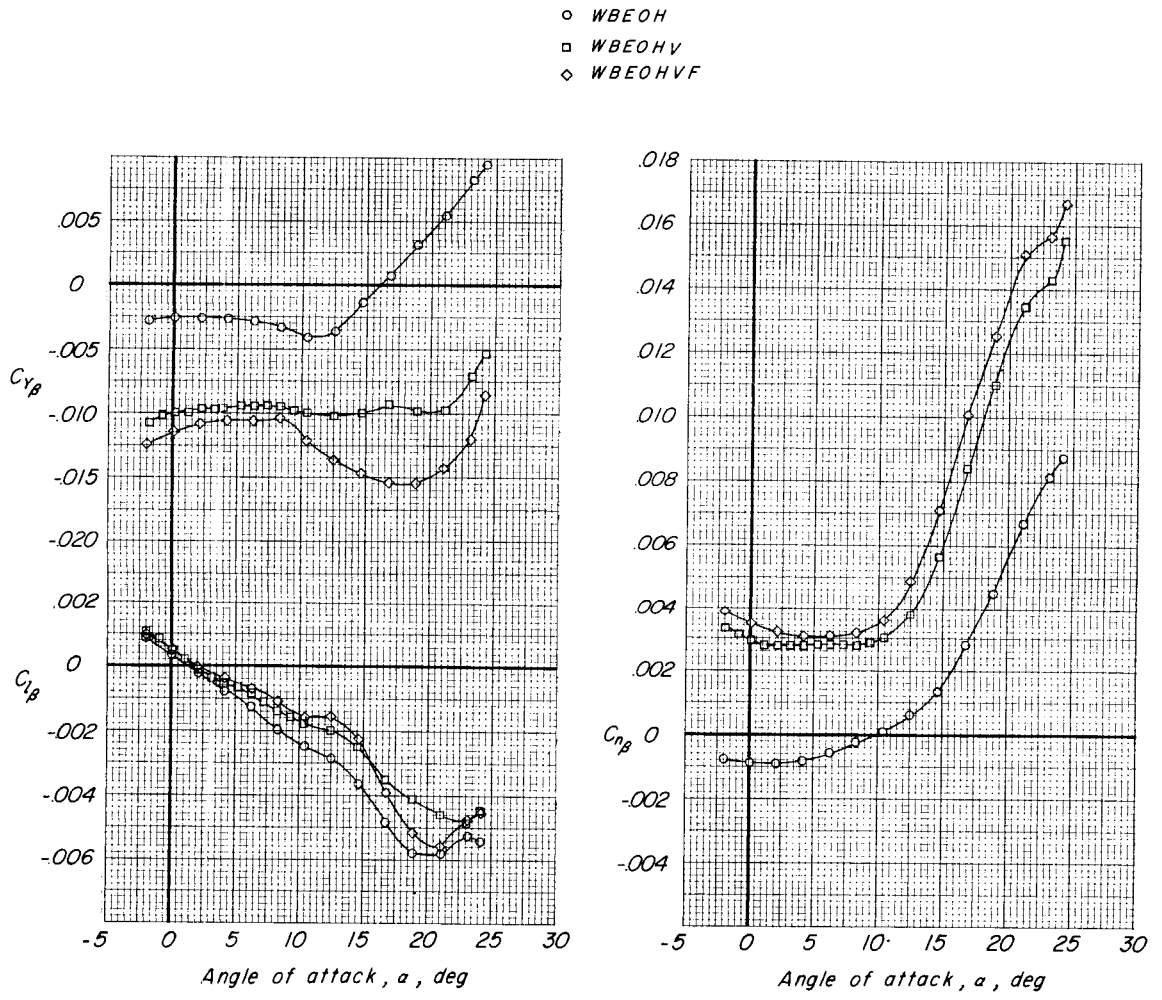

(a) M = 0.60.

Figure 13.- Effect of vertical tails and ventral fins on the static lateral-stability derivatives of model 1.

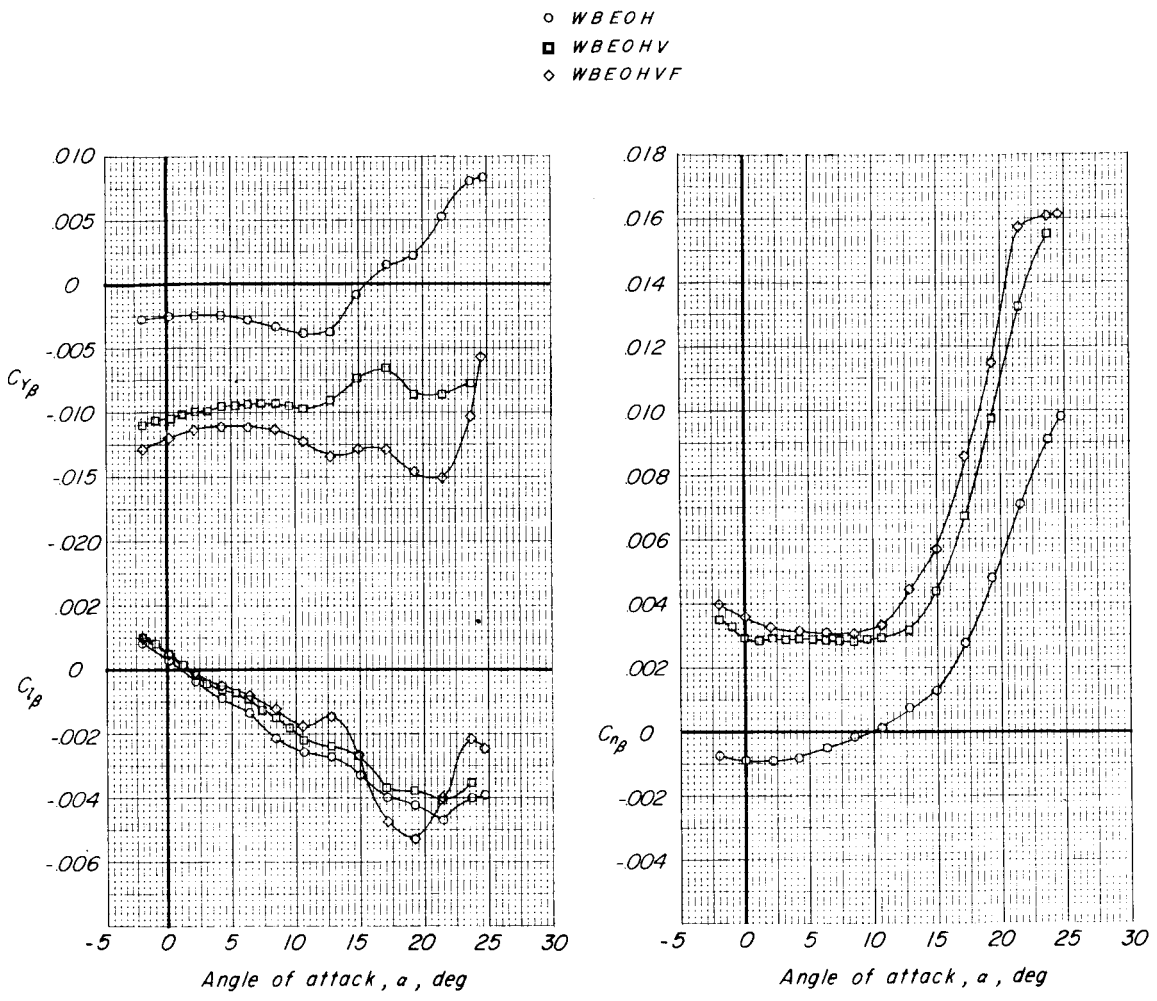

(b) M = 0.80.

Figure 13.- Continued.

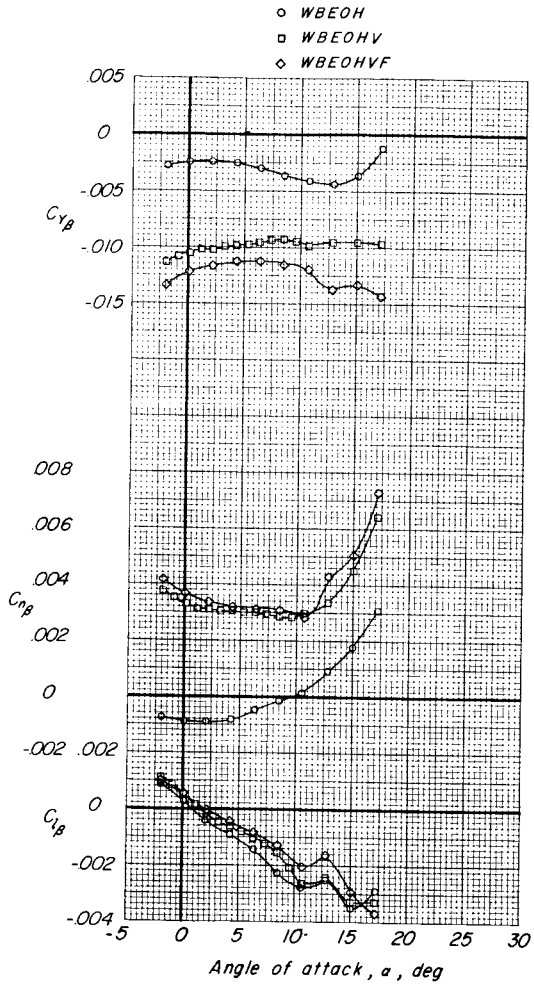

(c) M = 0.90.

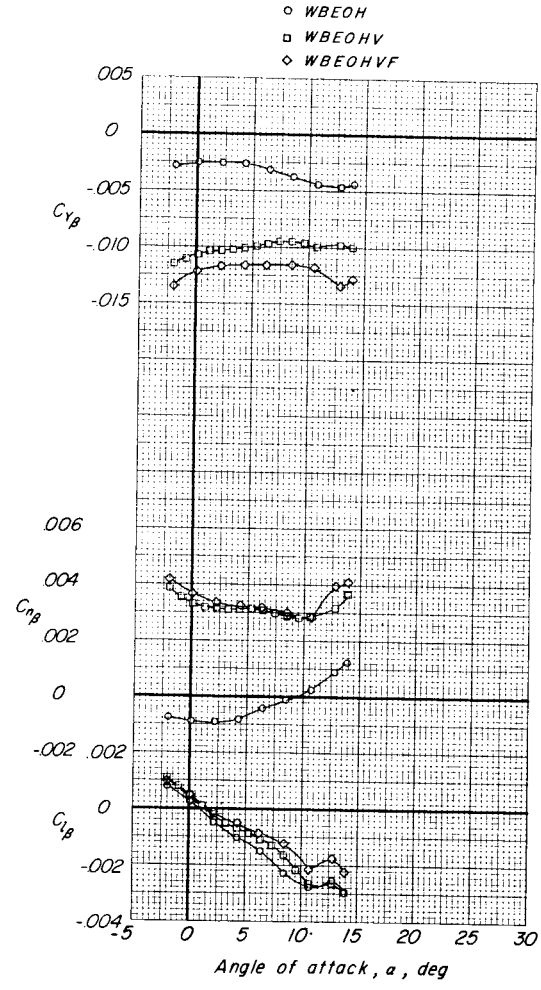

(d) M = 0.94.

Figure 13.- Concluded.

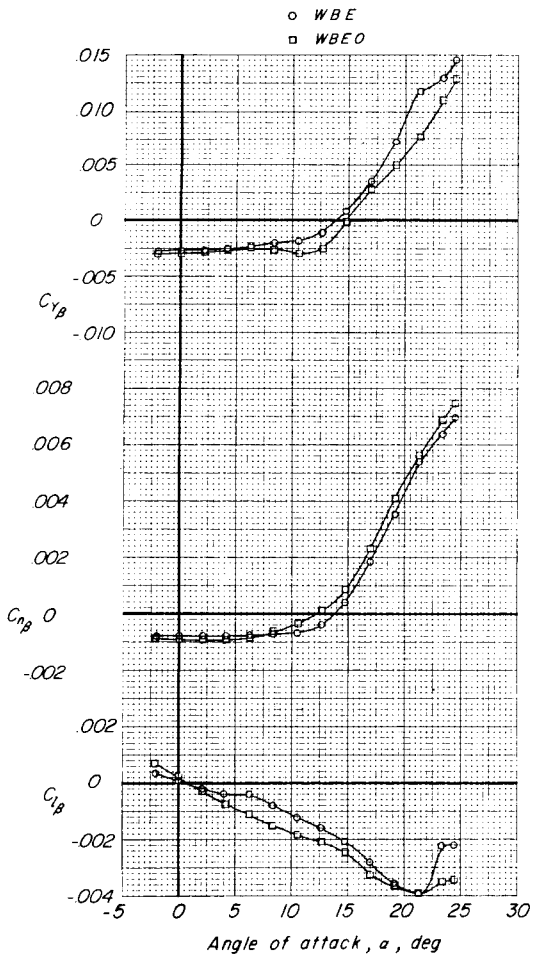

(a) M = 0.60.

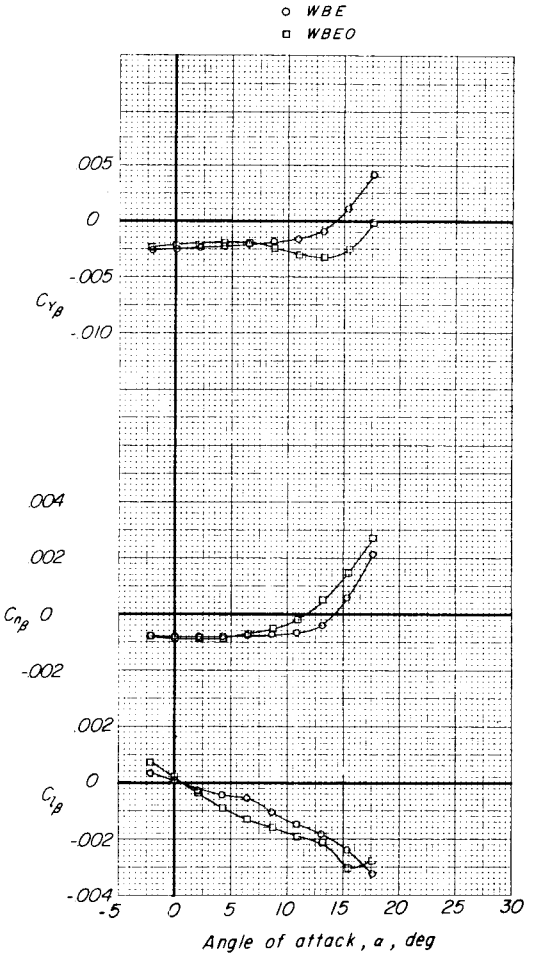

(b) M = 0.90.

Figure 14.- Effect of wingtip bodies on the static lateral-stability derivatives of model 1 with the horizontal tail removed.

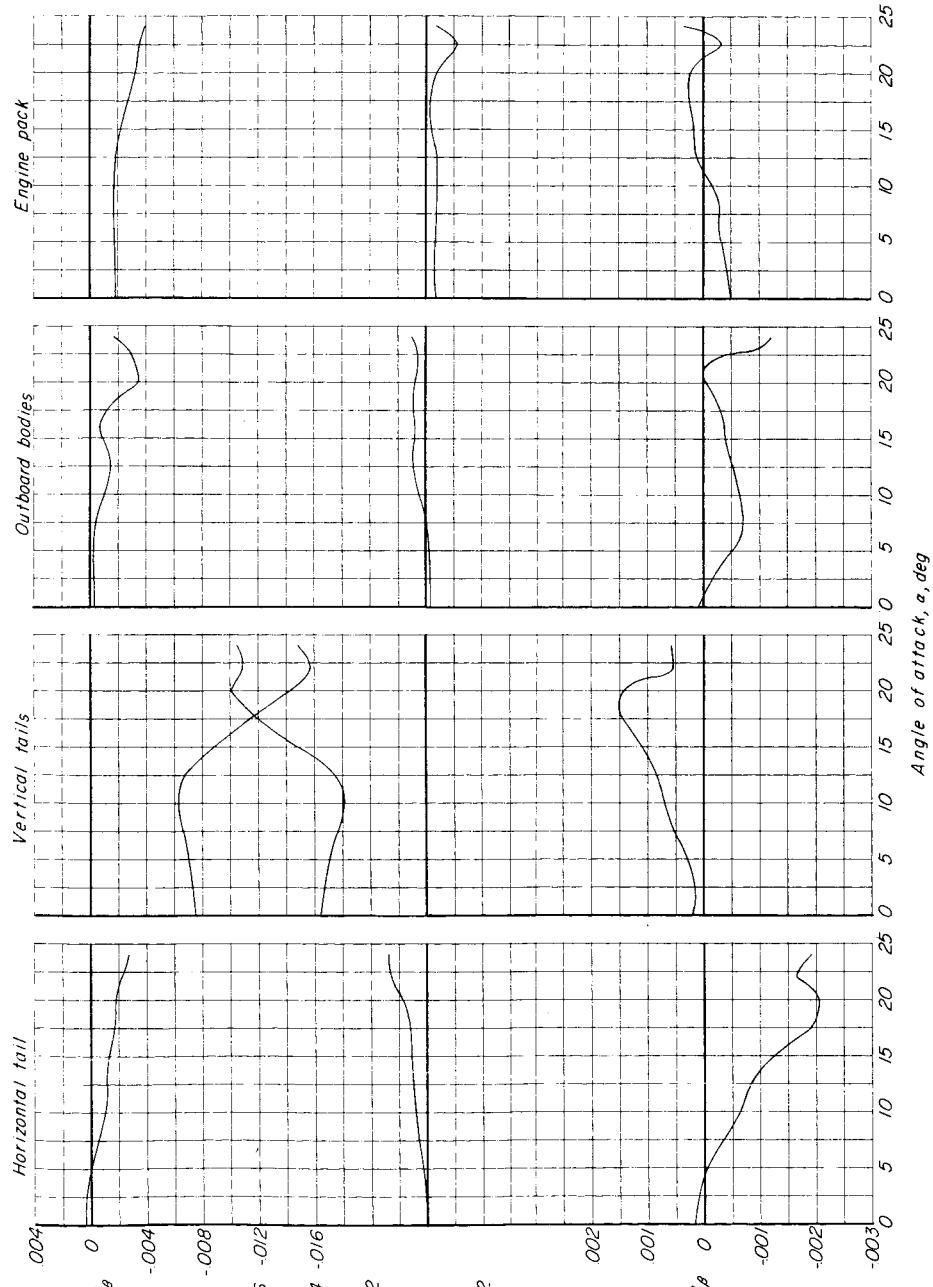

Figure 15.- Component contributions to static lateral-stability derivatives of model 1. $i_t = -0.1^\circ$ for results with horizontal tail on.

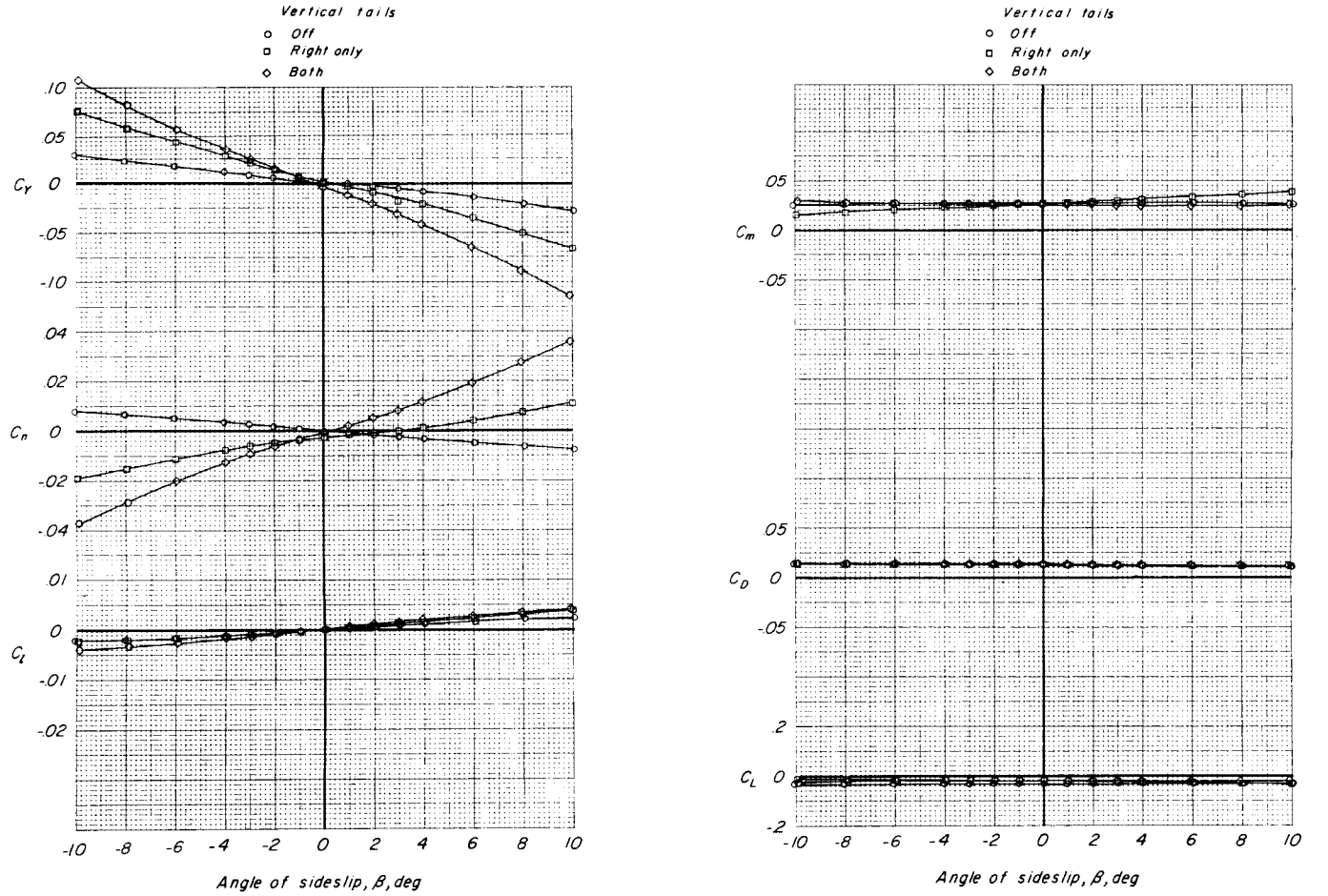

(a) M = 0.60; α = 0.04°.

Figure 16.- Effect of adding the right vertical tail surface and both vertical tail surfaces on the aerodynamic characteristics in sideslip of model 1. Configurations WBEOVH and WBEOH; i_t = -0.1°.

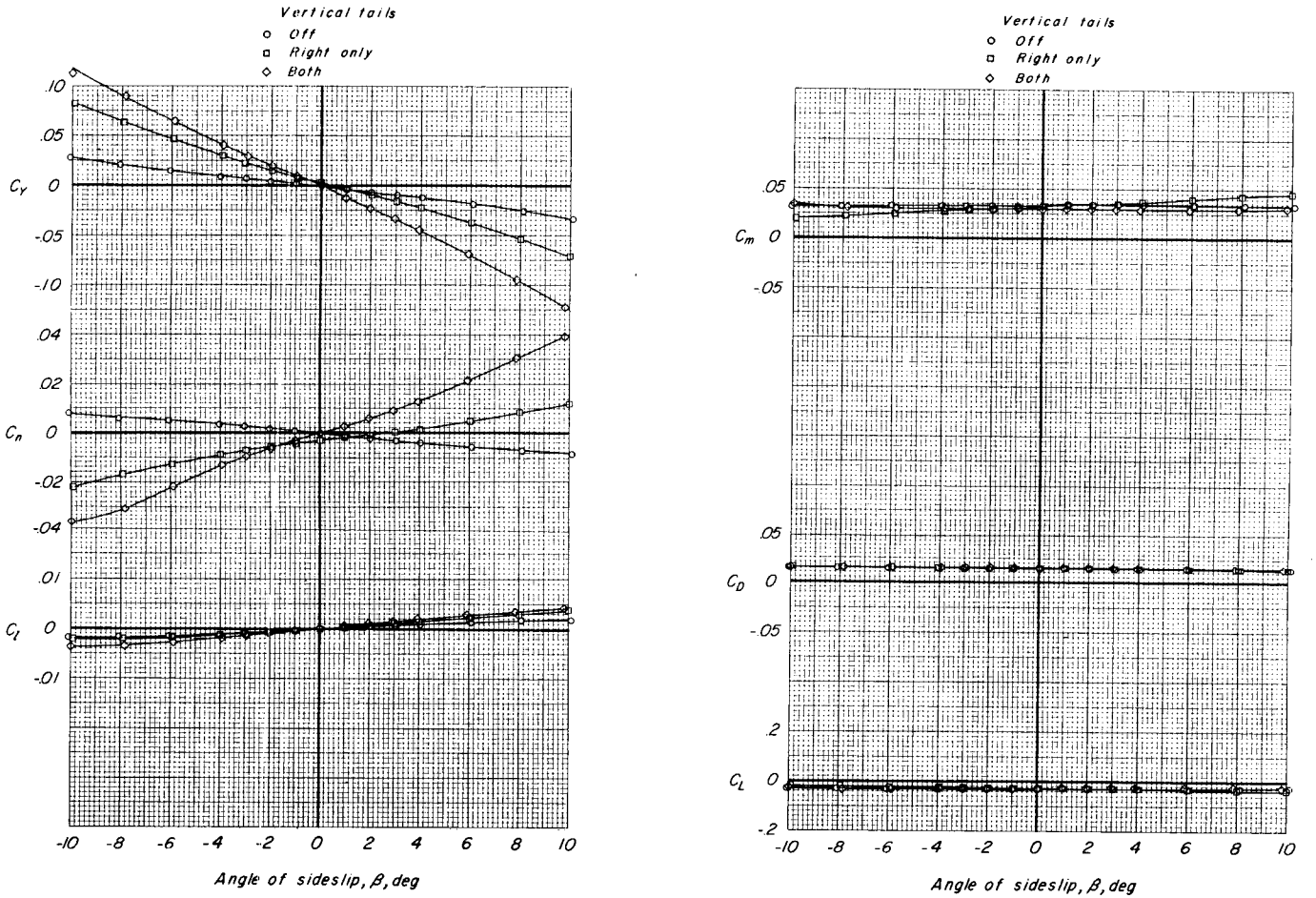

(b) M = 0.90; $\alpha = 0.08^{\circ}$.

Figure 16.- Continued.

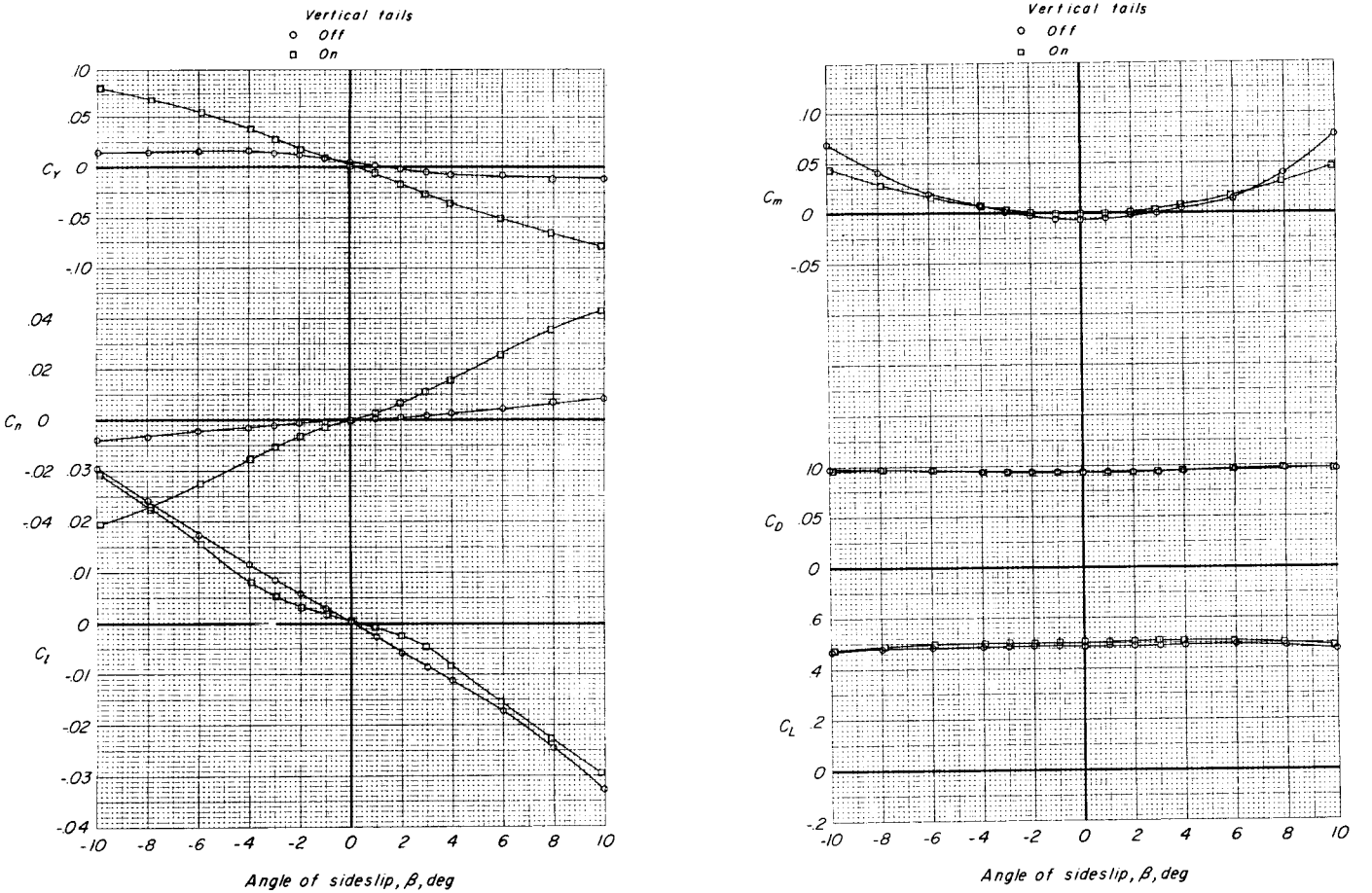

(c) M = 0.60; α = 12.47°.

Figure 16.- Continued.

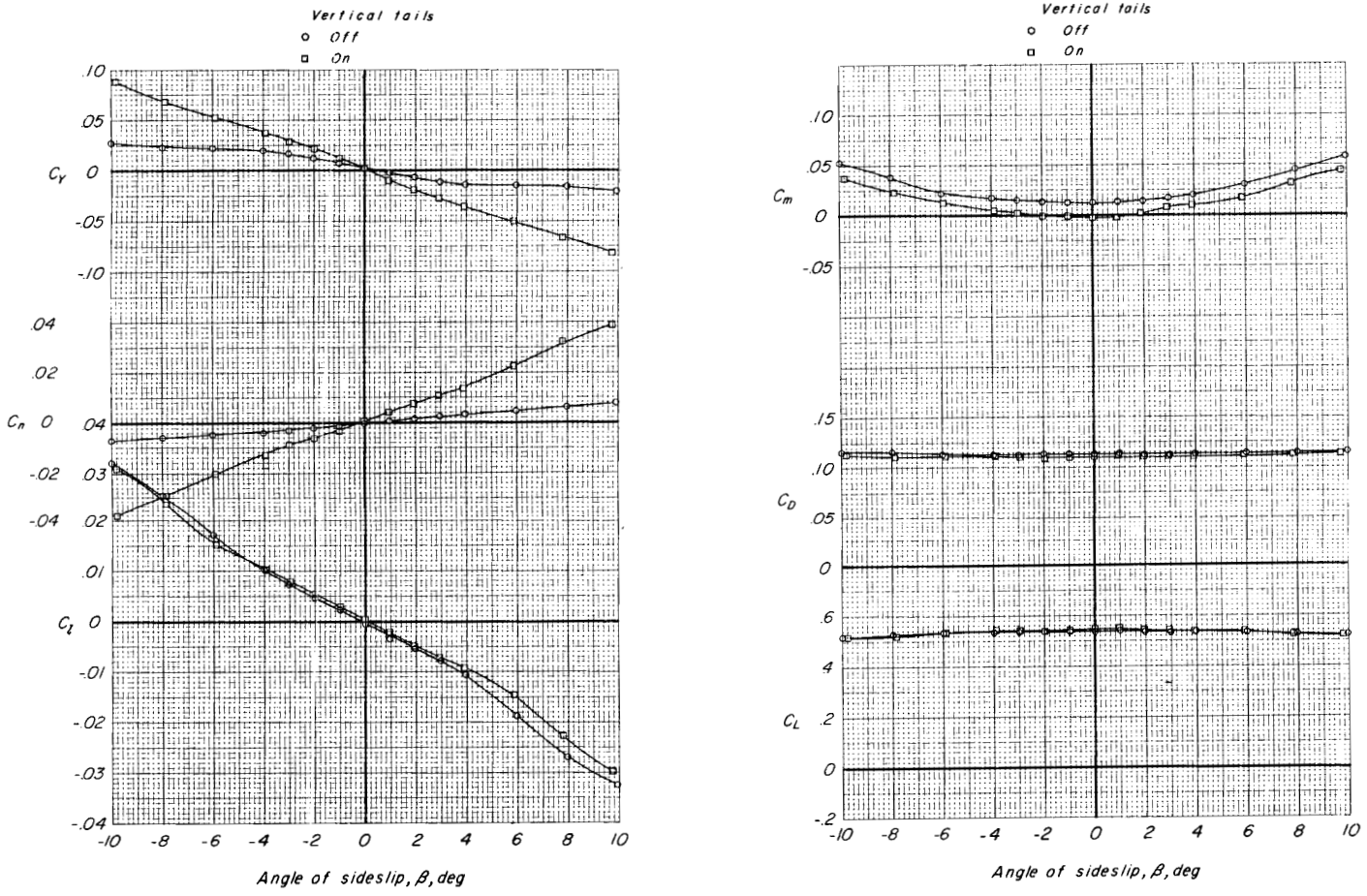

(d) M = 0.90; α = 12.82°.

Figure 16.- Continued.

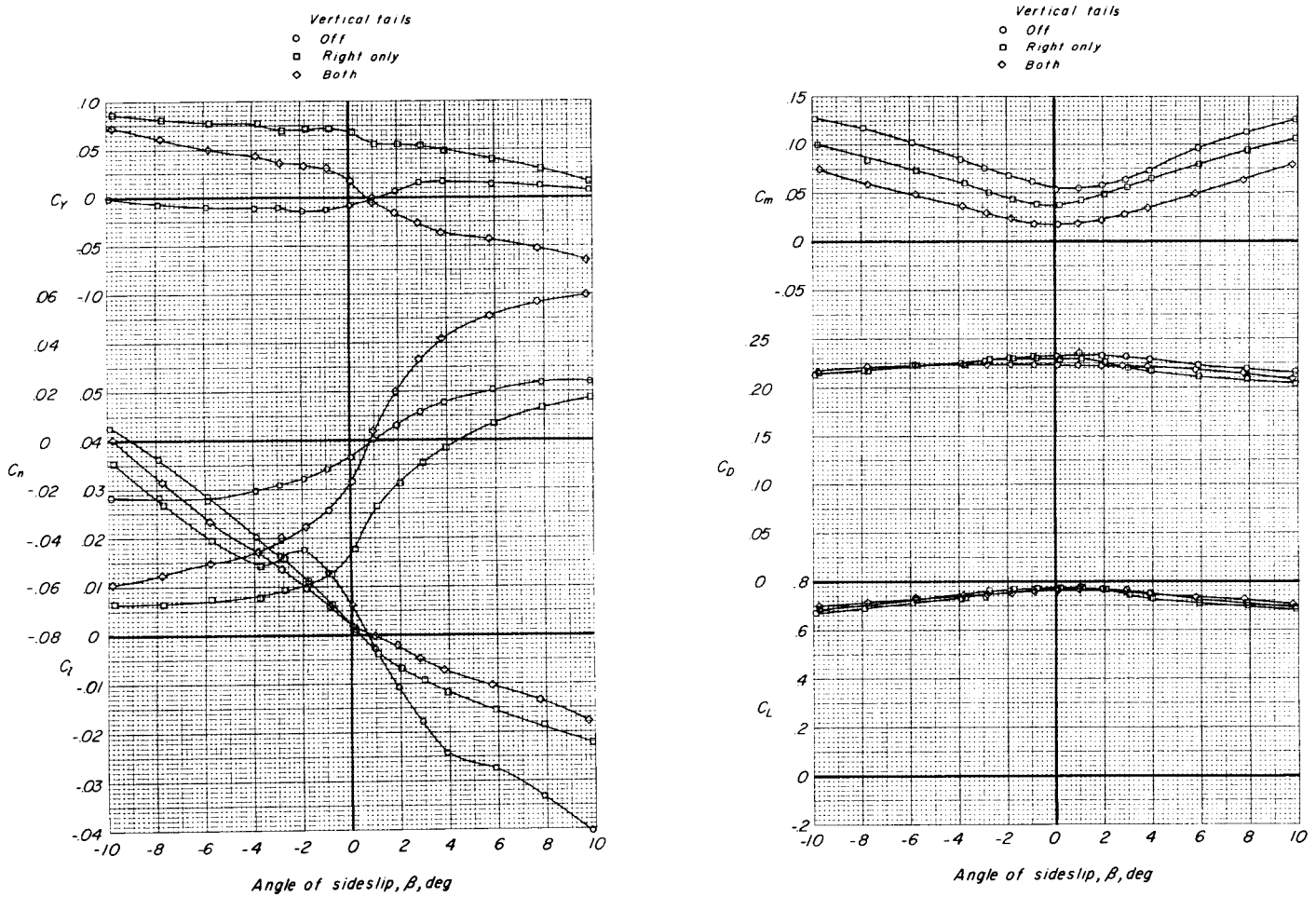

(e) M = 0.60; $\alpha = 18.78^{\circ}$.

Figure 16.- Concluded.

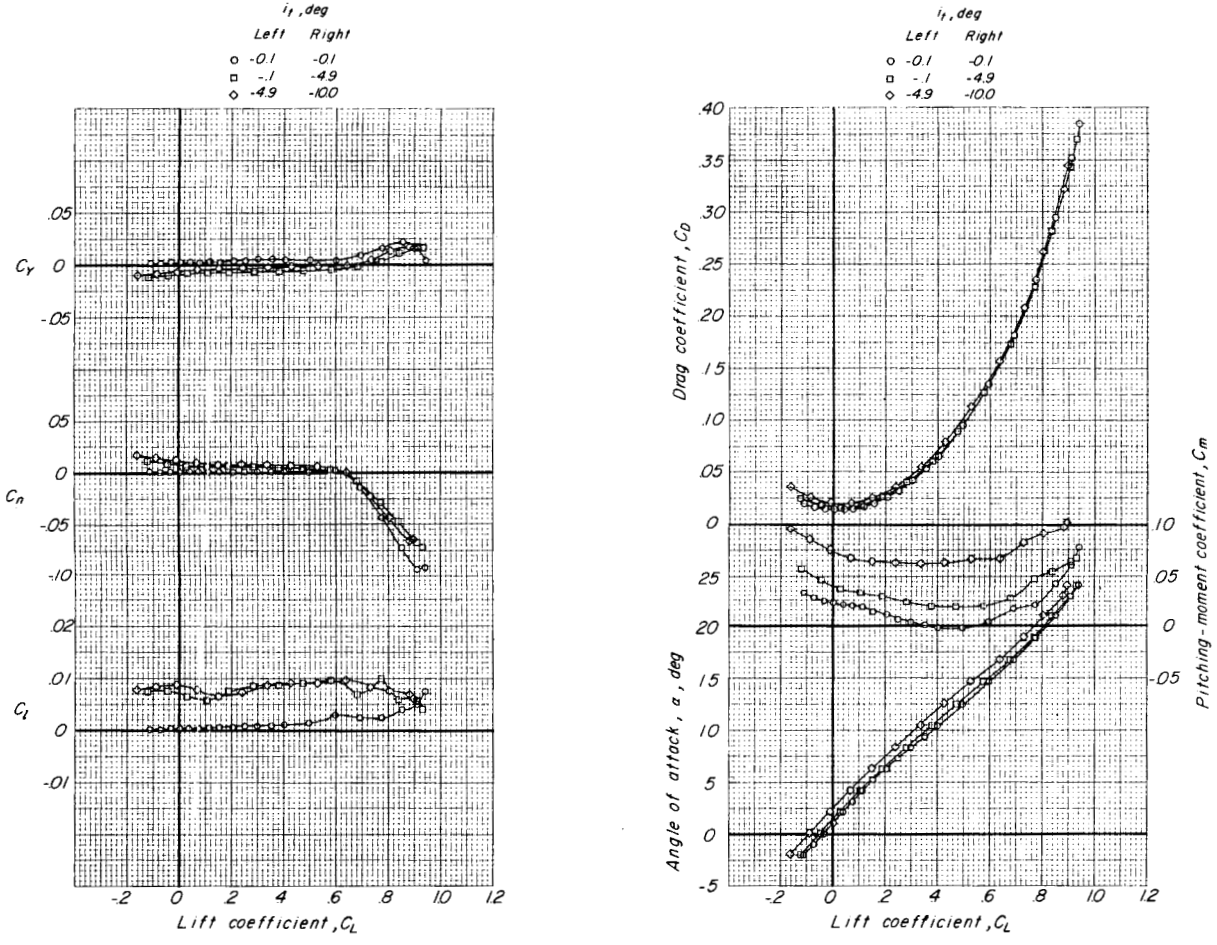

(a) M = 0.60.

Figure 17.- Effect of asymmetric deflection of the horizontal tail used as a roll control on the aerodynamic characteristics of model 1. Configuration WBEOVH.

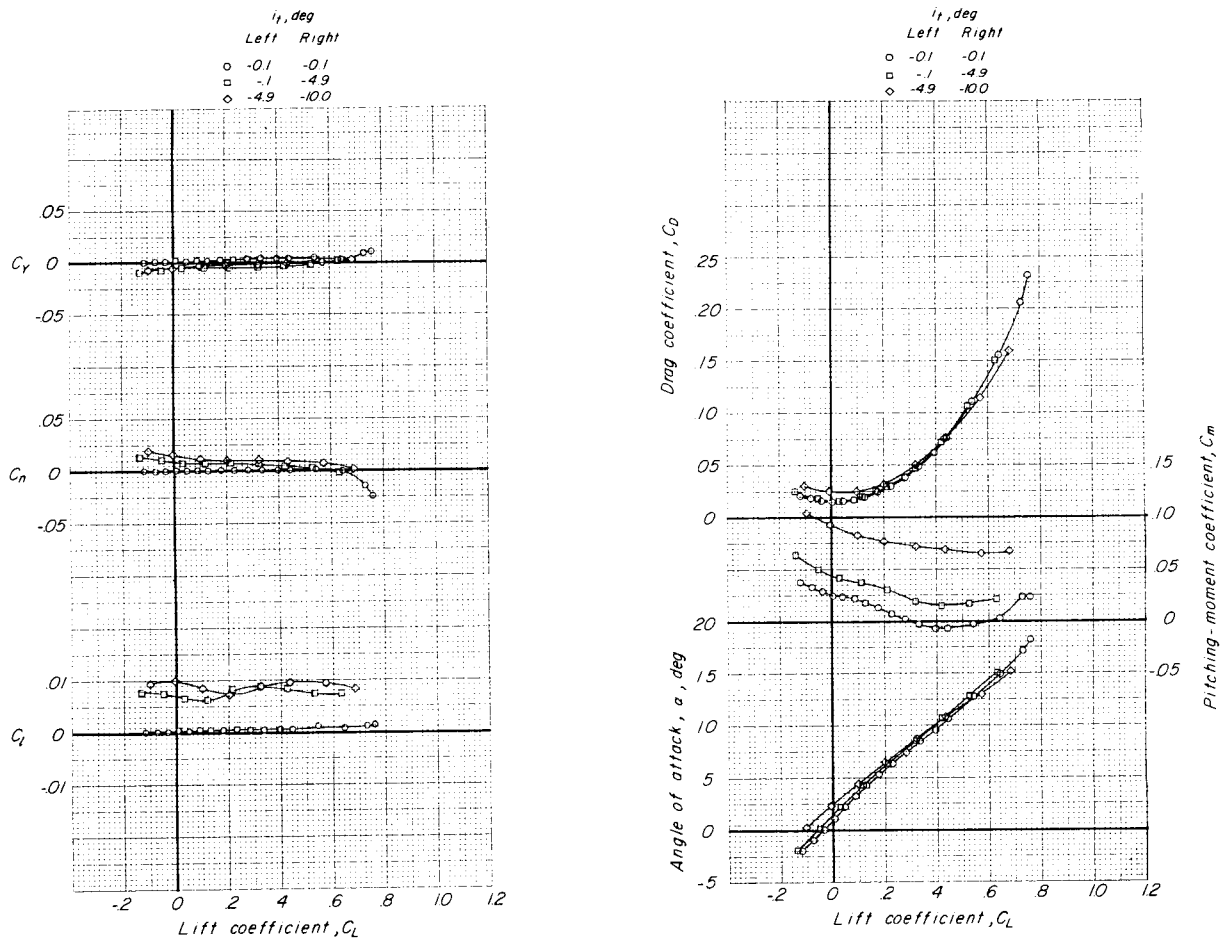

(b) M = 0.90.

Figure 17.- Concluded.

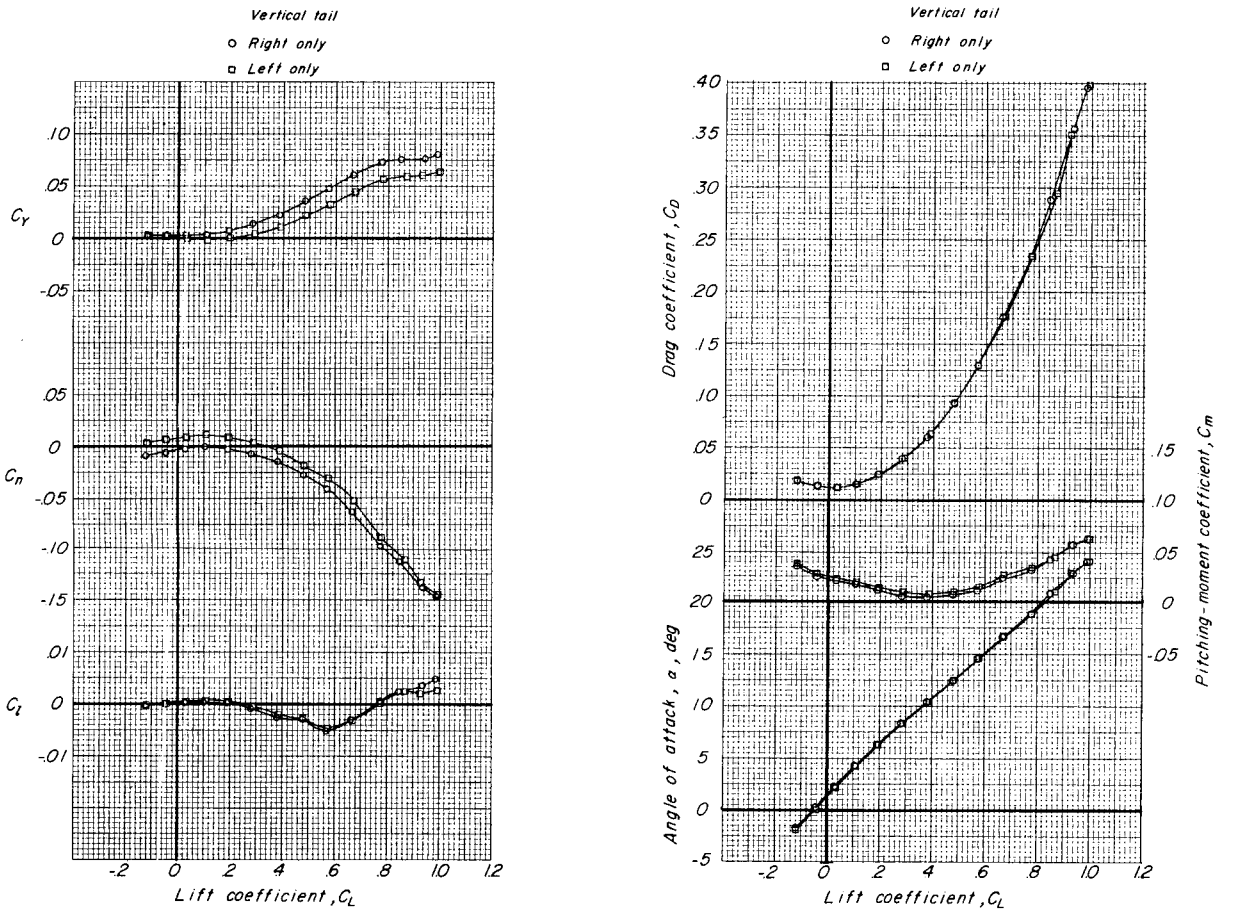

(a) M = 0.60.

Figure 18.- Effect of vertical-tail incidence on aerodynamic characteristics in pitch of model 1. Configuration WBEOVH; $i_t = -0.1^\circ$. (See fig. 2(a) for incidence of vertical tails.)

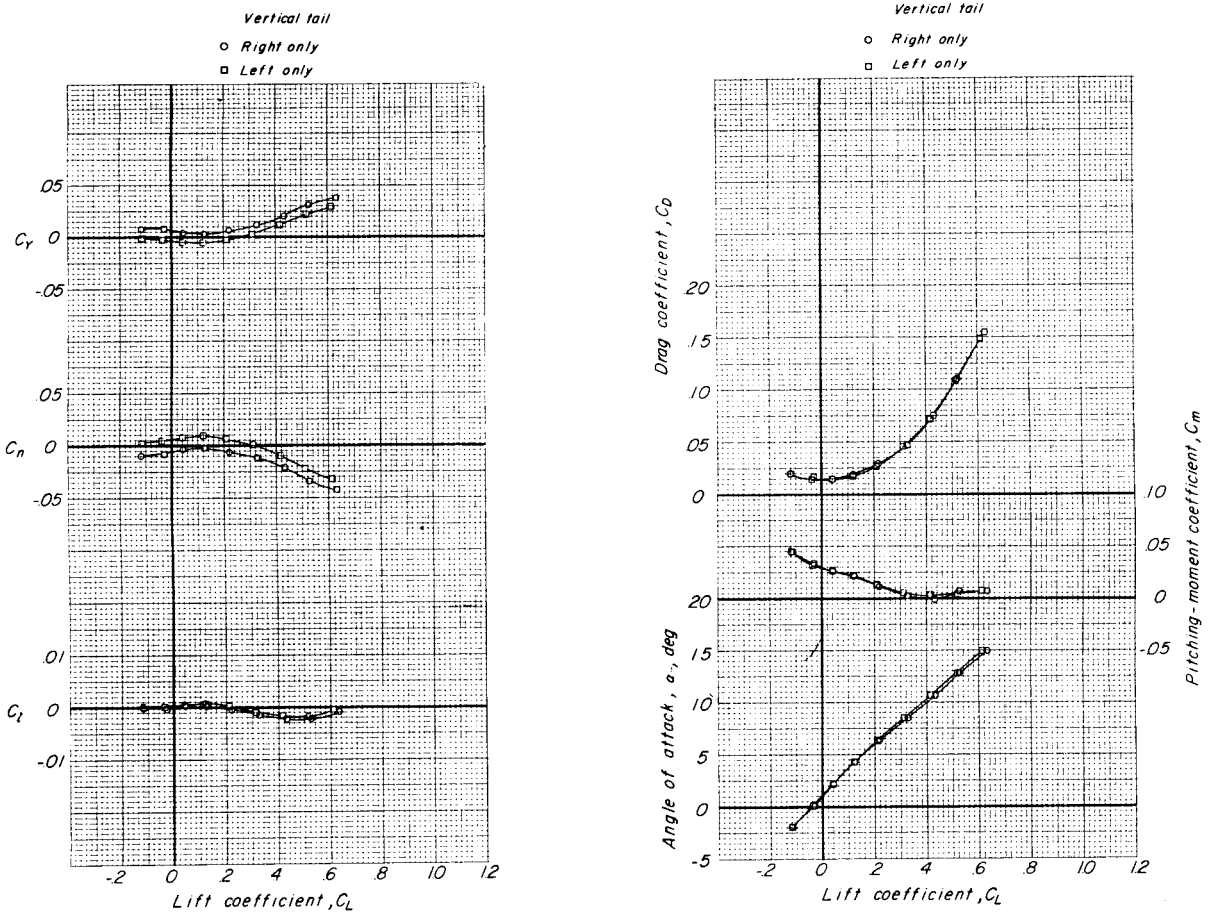

(b) M = 0.90.

Figure 18.- Concluded.

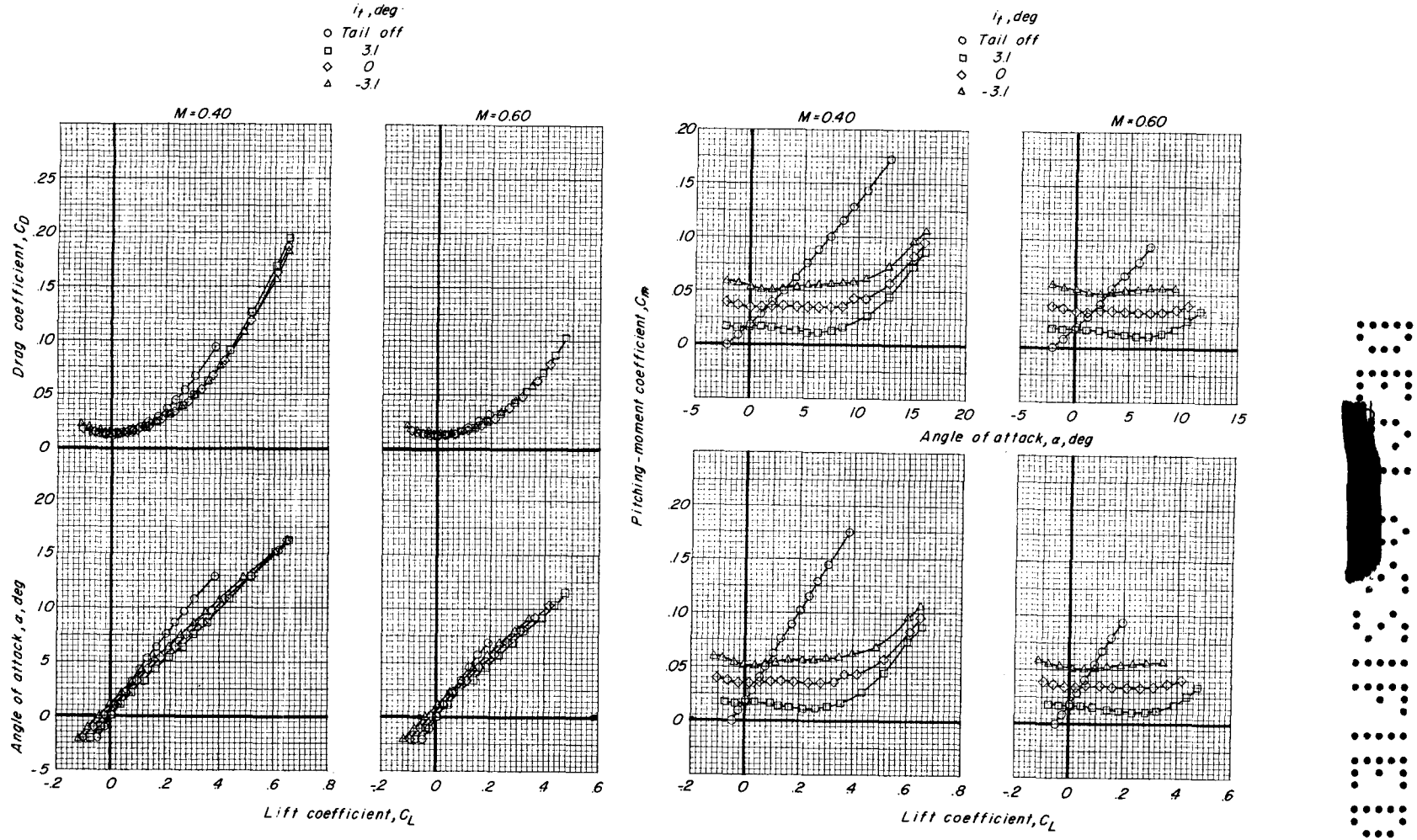

Figure 19.- Effect of horizontal-tail incidence on the longitudinal characteristics of model 2. Configuration WBEOVH.

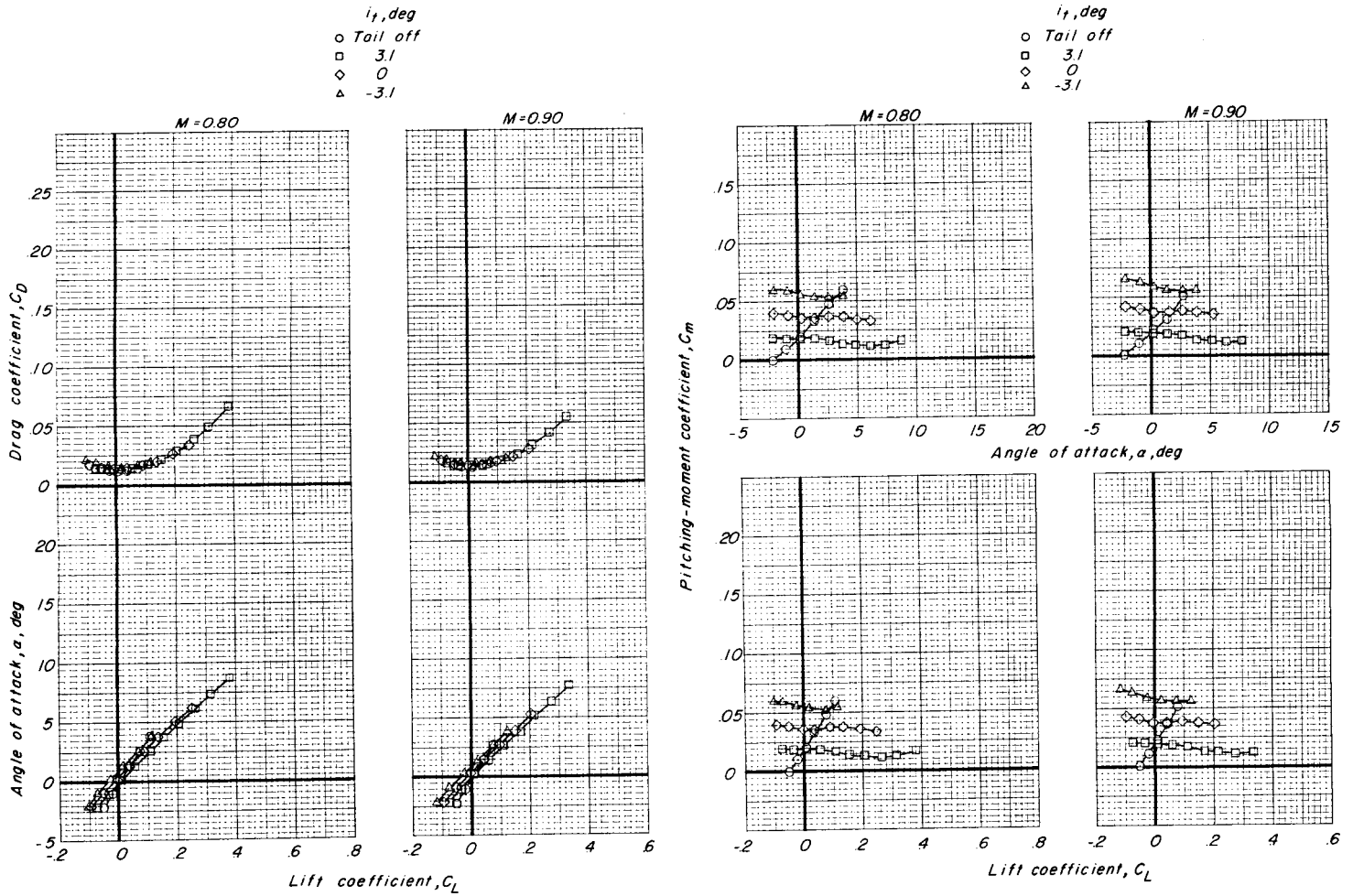

Figure 19.- Continued.

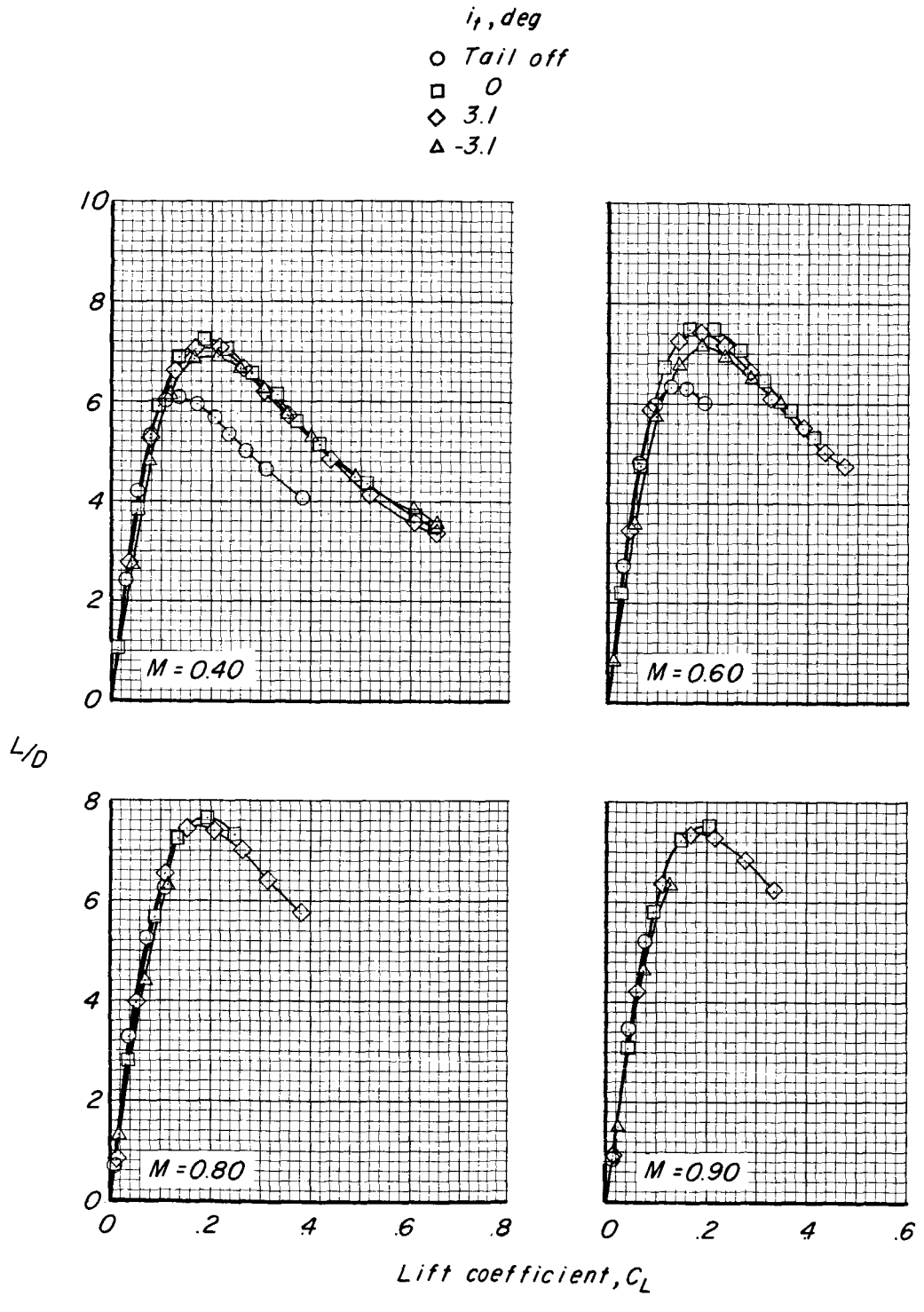

Figure 19.- Concluded.

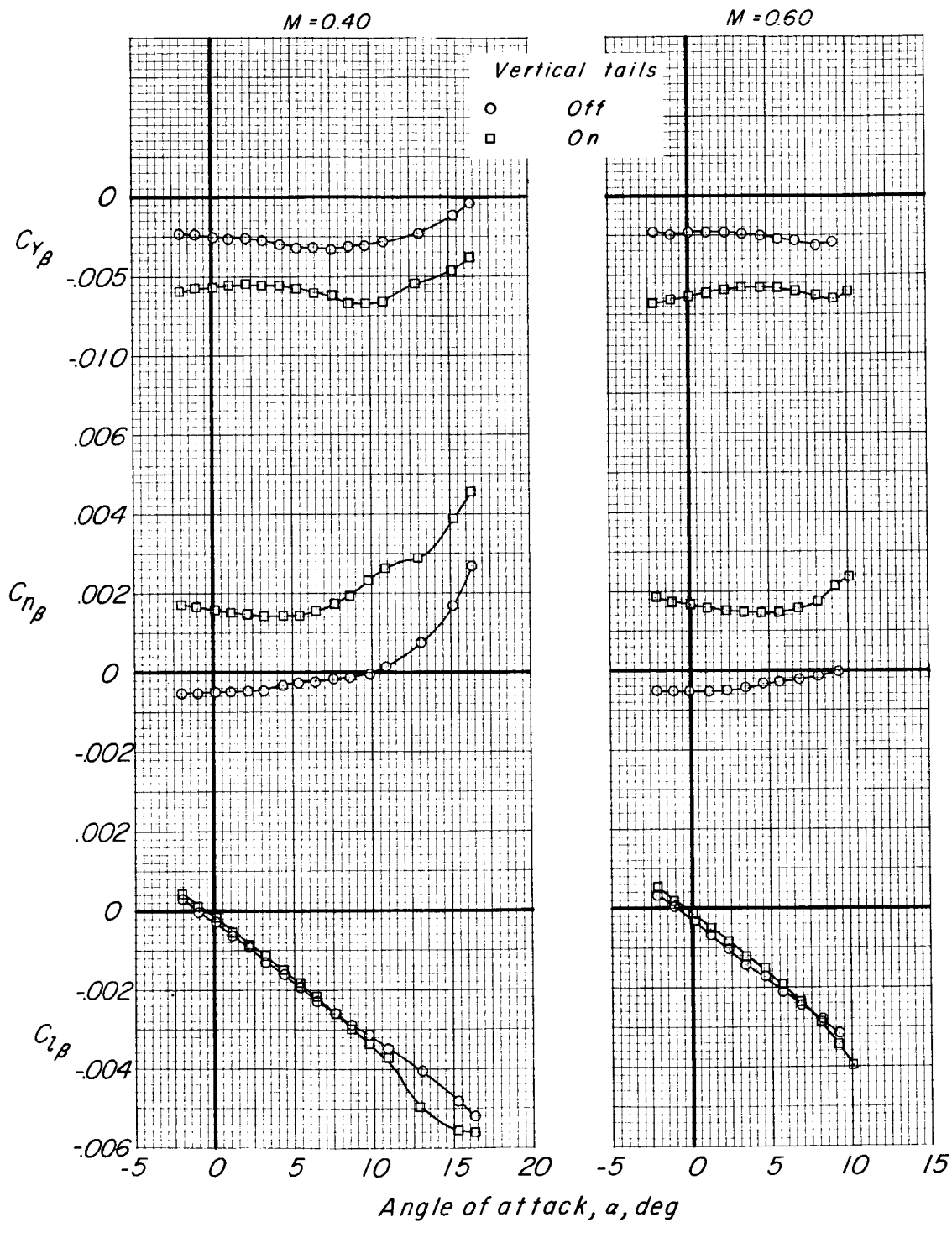

Figure 20.- Effect of vertical tails on the static lateral-stability derivatives of model 2. Configurations WBEOVH and WBEOH; $i_t = 3.1^\circ$.

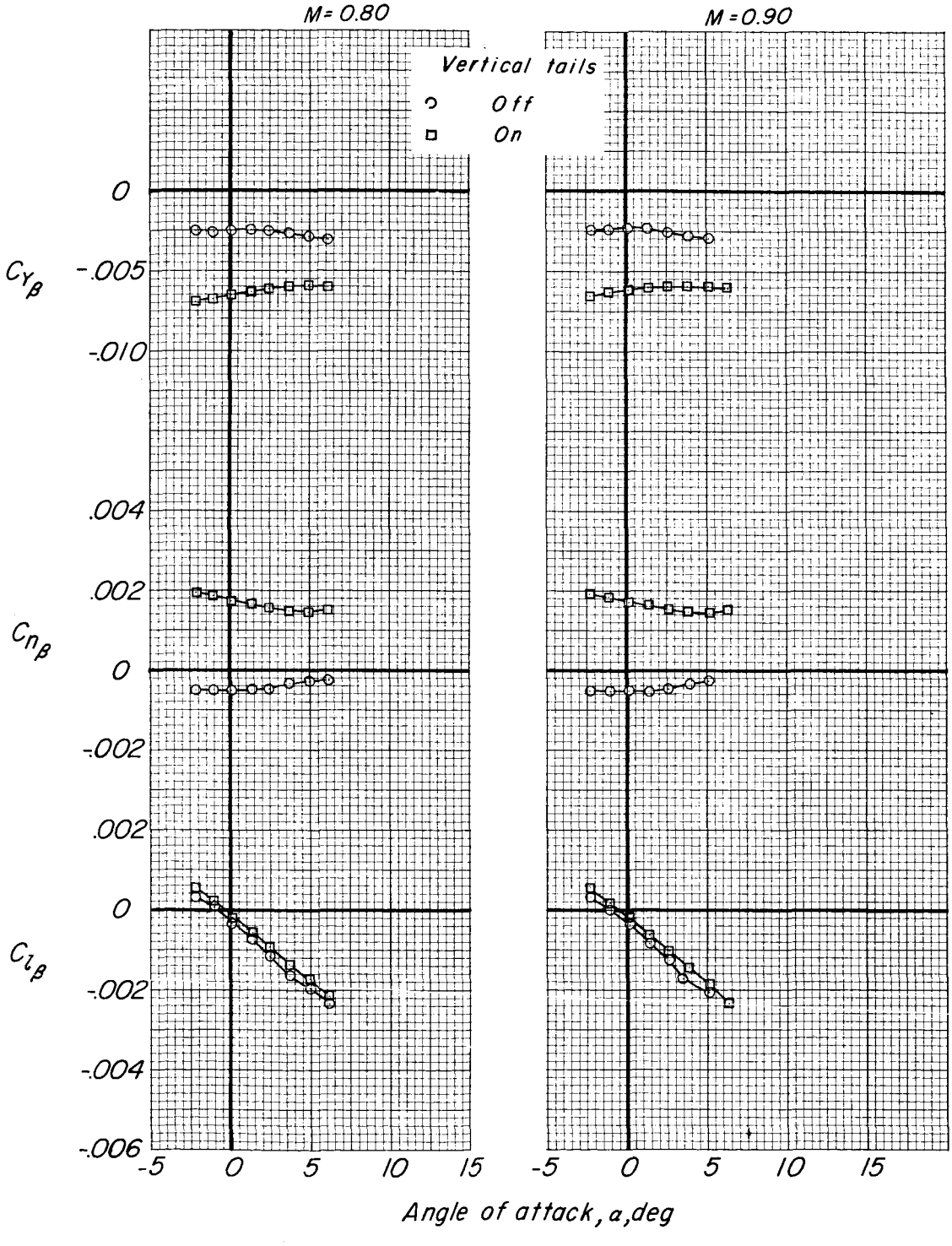

Figure 20.- Concluded.

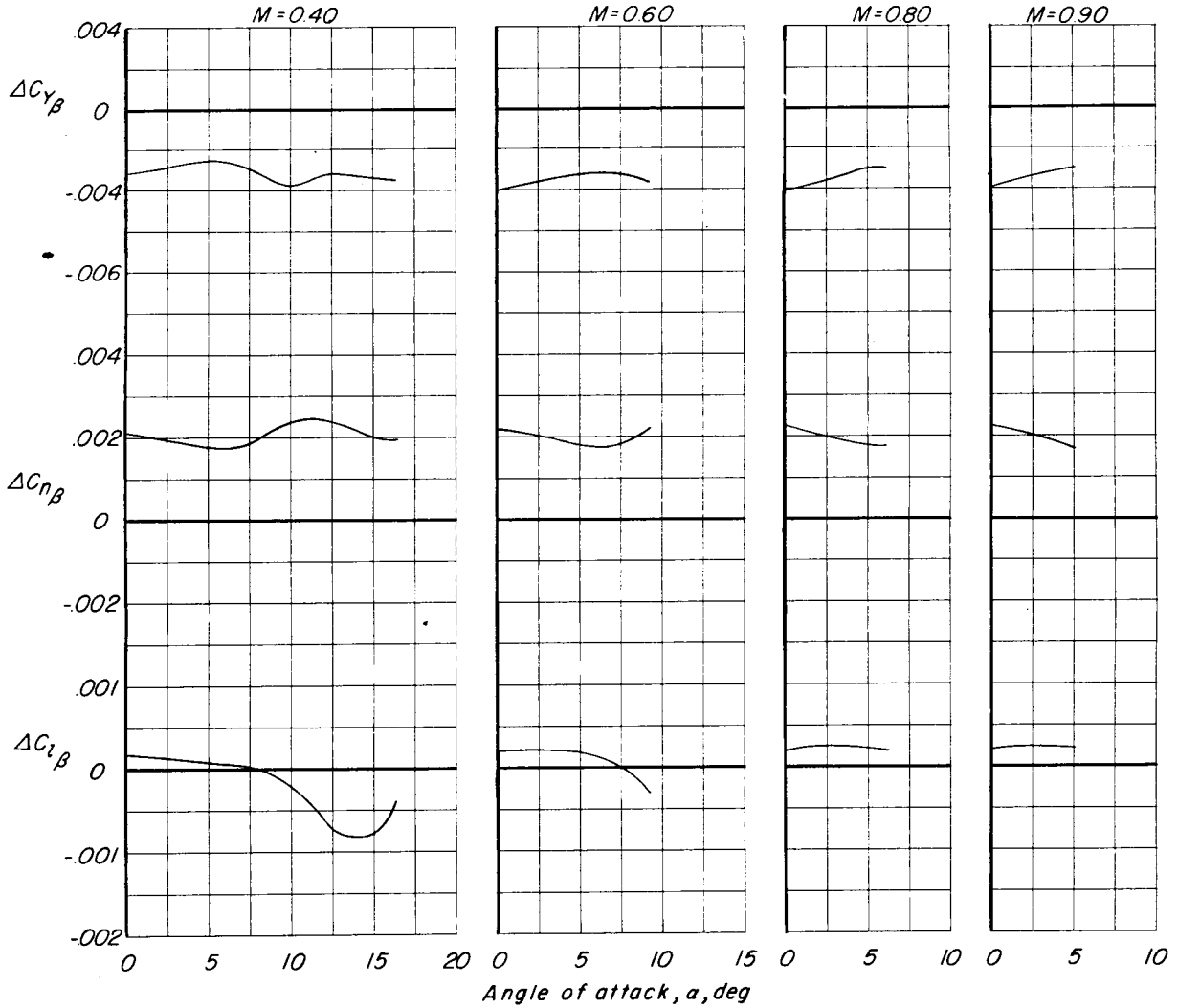

Figure 21.- Contribution of the vertical tails to the static lateral-stability derivatives of model 2.

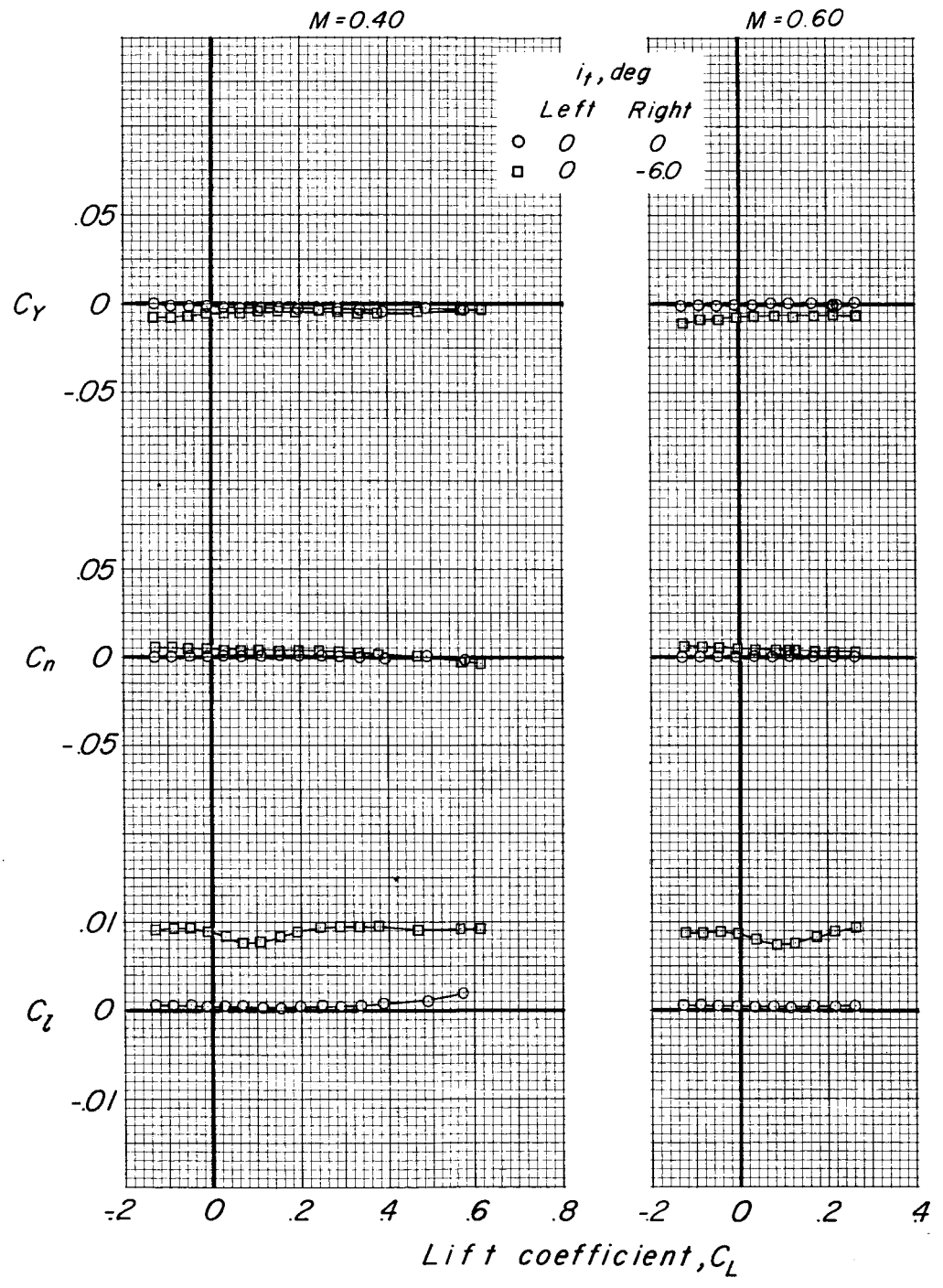

Figure 22.- Effect of asymmetric deflection of the horizontal tail used as a roll control on the aerodynamic characteristics of model 2. Configuration WBEOVH.

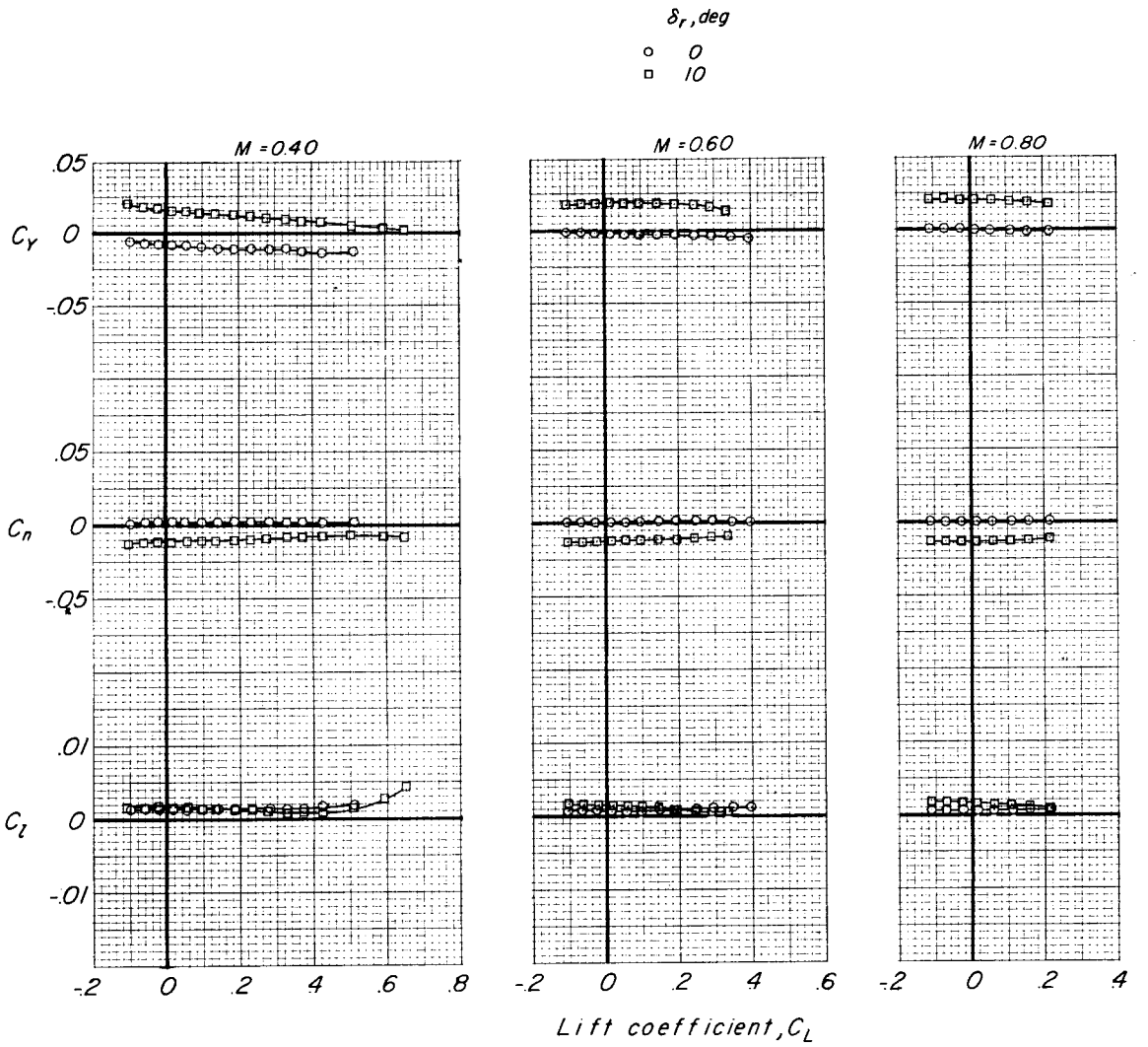

Figure 23.- Effect of rudder deflection on the lateral characteristics of model 2 at zero sideslip. Configuration WBEOVH; $i_t = 0^\circ$.

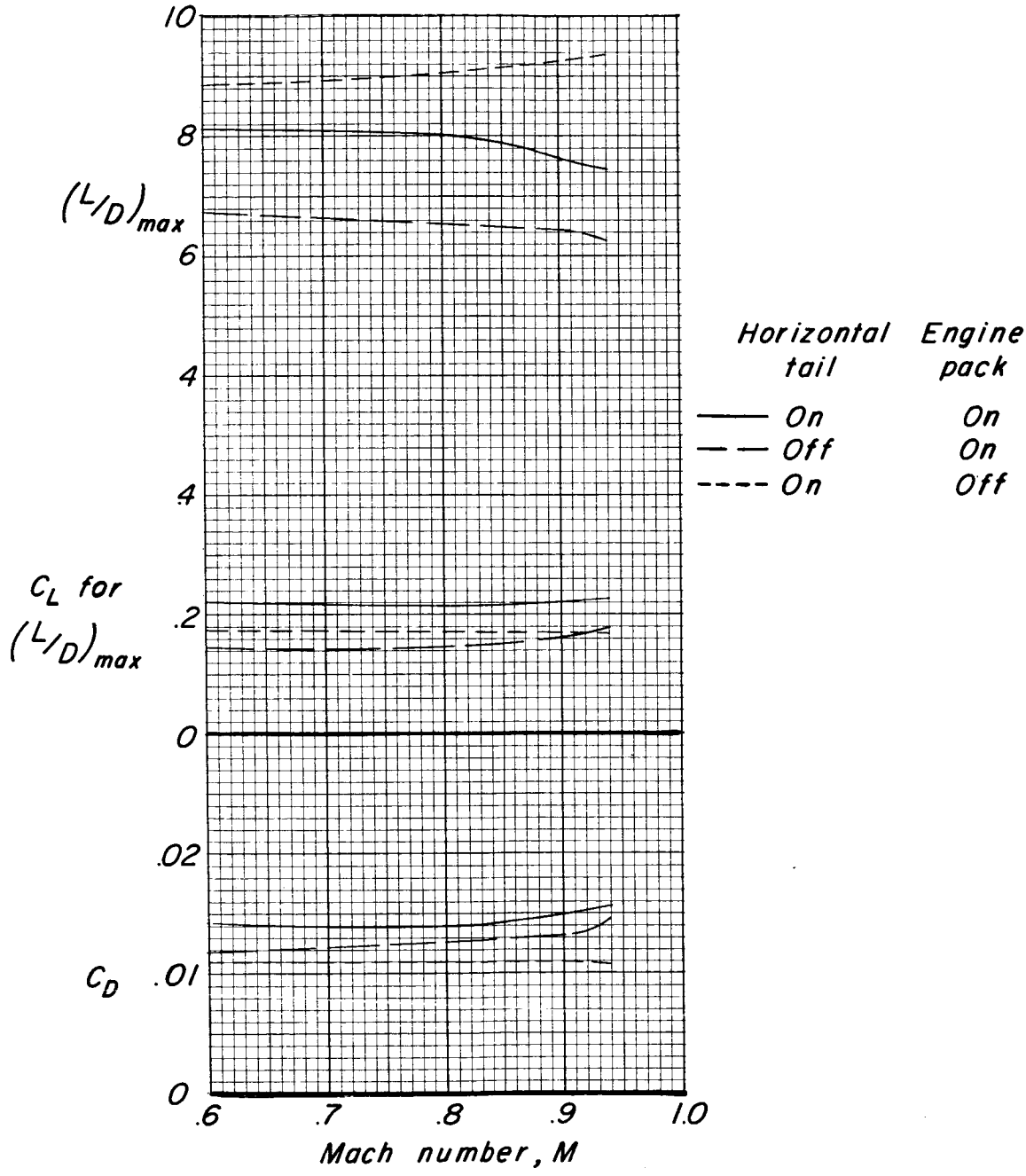

Figure 24.- Variation with Mach number of performance parameters of model 1.

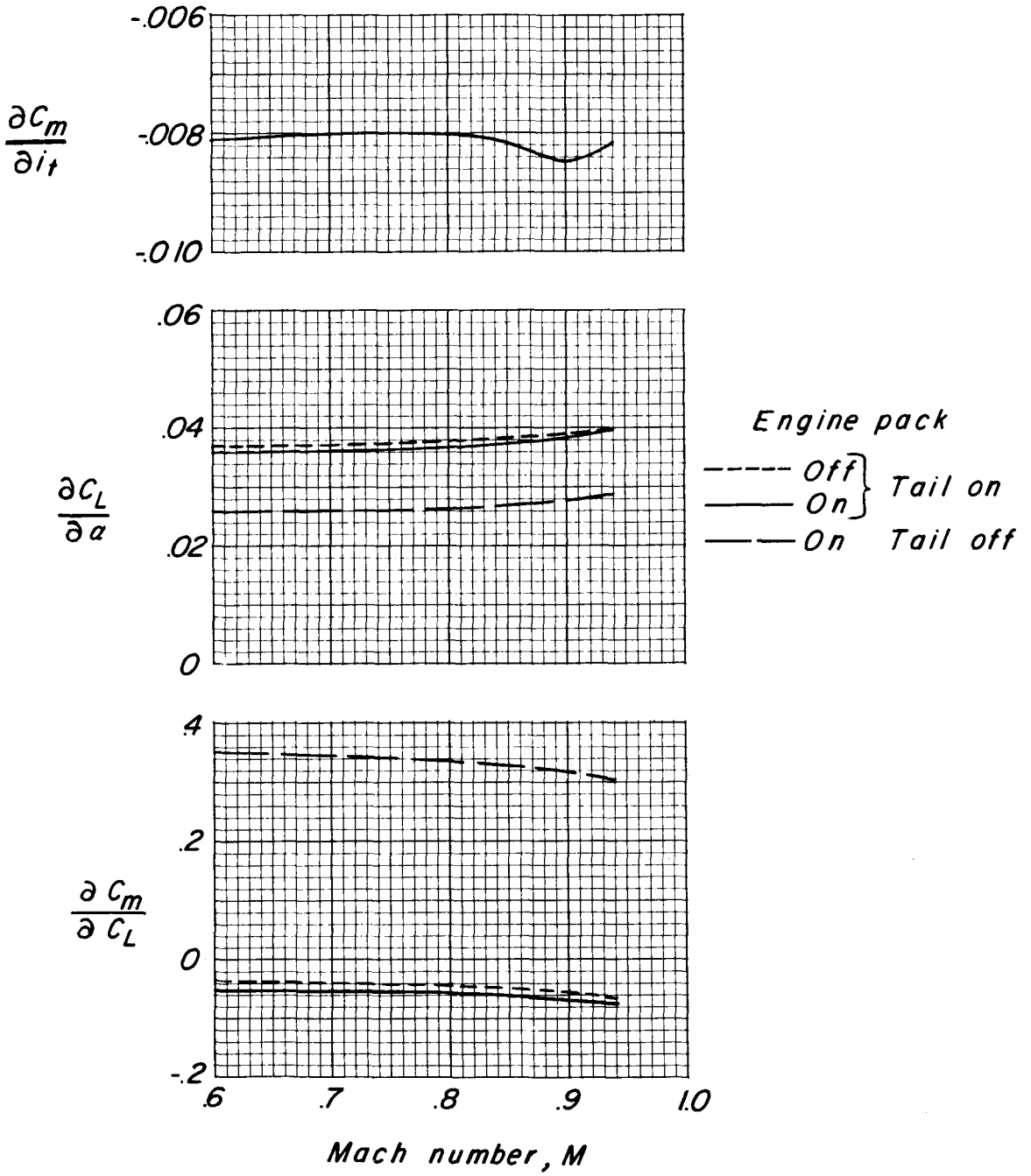

Figure 25.- Variation with Mach number of longitudinal-stability parameters of model 1.

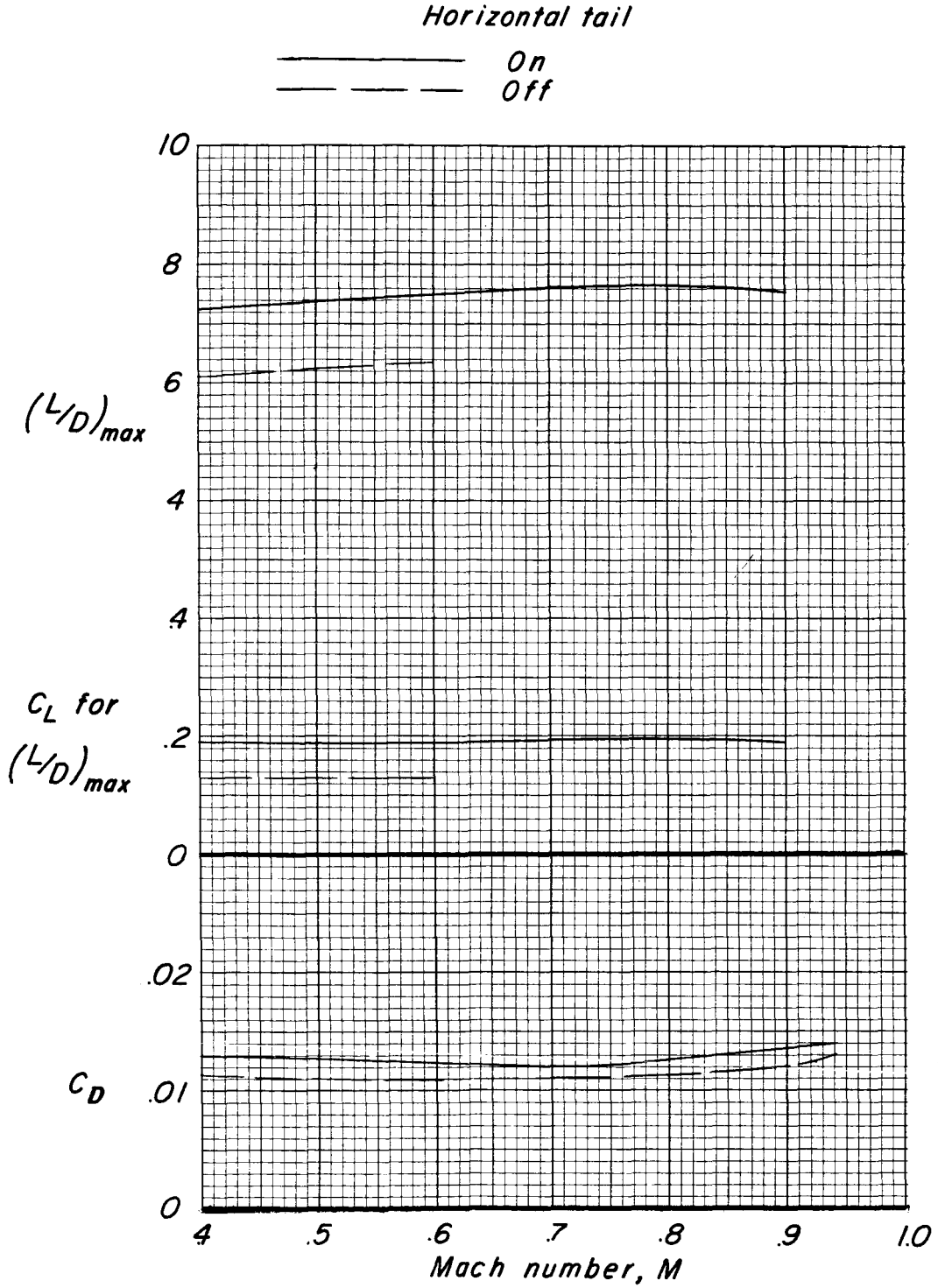

Figure 26.- Variation with Mach number of performance parameters of model 2.

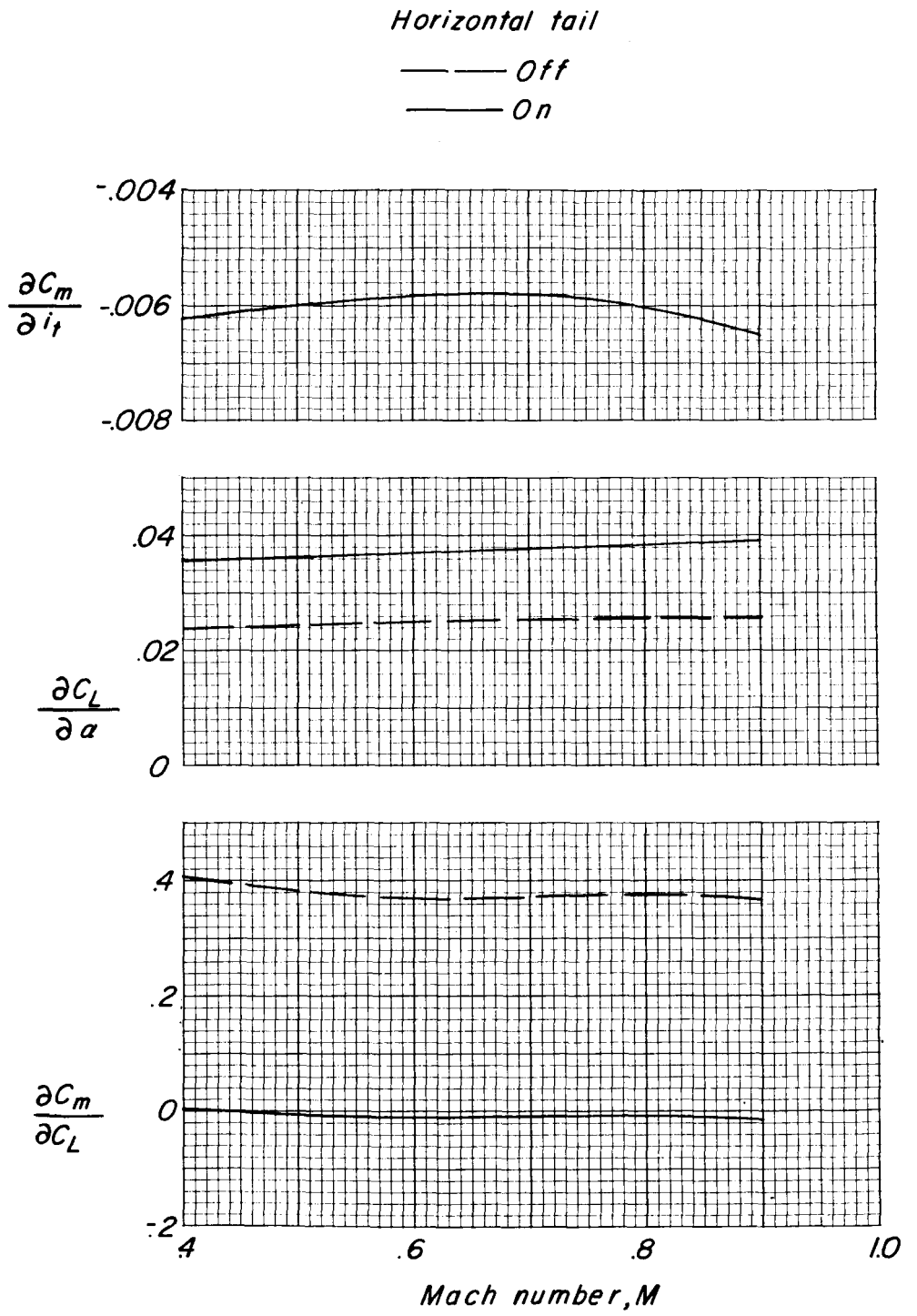

Figure 27.- Variation with Mach number of longitudinal-stability parameters of model 2.